

Contents lists available at ScienceDirect

Applied Numerical Mathematics

journal homepage: www.elsevier.com/locate/apnum





Computational wavefunction dynamics in photonic graphene with symmetry breaking



Emmanuel Lorin a,b,*, Xu Yang c

- ^a School of Mathematics and Statistics, Carleton University, Ottawa, K1S 5B6, Canada
- ^b Centre de Recherches Mathématiques, Université de Montréal, Montréal, H3T 1J4, Canada
- ^c Department of Mathematics, University of California, Santa Barbara, CA 93106, USA

ARTICLE INFO

Article history: Received 28 September 2022 Received in revised form 6 March 2023 Accepted 27 May 2023 Available online 21 June 2023

Keywords: Photonic graphene Edge state propagation Pseudospectral method Perfectly matched layers Schrödinger equation

ABSTRACT

This paper is devoted to the derivation and analysis of a simple pseudospectral computational method for a two-dimensional time-dependent Schrödinger equations with periodic coefficients, modeling electromagnetic waves propagating in photonic graphene with symmetry breaking. In particular, we are interested in the propagation of edge states along a wall, modeling a defect/heterogeneity in the optical set-up. Perfectly matched layers are here combined with the derived pseudospectral method in order to absorb wavefunctions in the direction orthogonal to the wall. We numerically and analytically exhibit the possible trapping of wavefunctions.

© 2023 IMACS. Published by Elsevier B.V. All rights reserved.

1. Introduction

The dynamical phenomena on photonic graphene and more generally photonic topological insulators are become a very active research field [27] with recent and unexpected discoveries. The study of photonic graphene allows to explore optoelectronic devices and more generally the fundamental topological properties of optical systems with application to topological lasers (allowing protected transport, edge state propagation) singular optical beams, and spin-orbit coupling. Let us mention a recent work [20], where thermalized states and topological edge flow in two-dimensional nonlinear topological insulators on Haldane lattices are described by a normalized discrete nonlinear Schrödinger equation. Long range interactions were also analyzed in [23]. In practice, photonic graphene sets-up coupled waveguides, microwave resonators, nonlinear crystals, atomic vapor cells, see [33] for references. The dynamics of electromagnetic waves on photonic graphene is primarily modeled using Maxwell's equations, but some standard hypotheses (paraxial approximation, slowly varying envelop approximation, etc.) often lead to simple nonlinear Schrödinger equations on honeycomb lattices. Paraxial discrete Schrödinger equation can also be used, see [26]. In this present paper, we will consider more accurate linear Schrödinger's models with non-constant coefficients, derived from Maxwell's equations.

In this paper, we are interested in the propagation of electromagnetic waves in photonic graphene [19,21,24–26,32], in particular when some symmetry properties in the material are broken. For instance in this case, it is well-known that the so-called edge states can be captured and propagate "along" walls or domain boundaries [22]. In general, photonic graphene is geometrically modeled by a honeycomb lattice Λ , defined by

E-mail addresses: elorin@math.carleton.ca (E. Lorin), xuyang@math.ucsb.edu (X. Yang).

^{*} Corresponding author.

$$\Lambda = \mathbb{Z} \boldsymbol{v}_1 \oplus \mathbb{Z} \boldsymbol{v}_2.$$

generated by two vectors $\mathbf{v}_1 = (\sqrt{3}, 1)^T/2$, $\mathbf{v}_2 = (\sqrt{3}, -1)^T/2$, and with dual lattice vectors $\mathbf{k}_1 = 2\pi (1, \sqrt{3})^T/\sqrt{3}$, $\mathbf{k}_2 = 2\pi (1, -\sqrt{3})^T/\sqrt{3}$ (see [22]):

$$\Lambda^* = \mathbb{Z} \mathbf{k}_1 \oplus \mathbb{Z} \mathbf{k}_2.$$

The so-called fundamental cell is defined by

$$\Omega := \left\{ \tau_1 \mathbf{v}_1 + \tau_2 \mathbf{v}_2 : \tau_i \in [0, 1), i = 1, 2 \right\}.$$

For $\Sigma := \mathbb{R}^2/\mathbb{Z} \mathbf{v}_1$, we define the domain

$$\Omega_{\Sigma} := \{ \tau_1 \mathbf{v}_1 + \tau_2 \mathbf{v}_2 : \tau_1 \in [0, 1], \tau_2 \in \mathbb{R} \},$$

and a truncated version, for some L > 0,

$$\Omega_{\Sigma : I} := \{ \tau_1 \mathbf{v}_1 + \tau_2 \mathbf{v}_2 : \tau_1 \in [0, 1], \tau_2 \in [-L, L] \}.$$

The evolution of wavefunctions in this material is modeled by a time-dependent Maxwell equations, which can be rewritten as a Schrödinger-like equation (see again [22] for details):

$$i\partial_t \psi = \mathcal{L}^{\delta} \psi$$
, where $\mathcal{L}^{\delta} := -\nabla \cdot (\boldsymbol{W}(\boldsymbol{x})\nabla)$, (1)

where the medium is described by a matrix valued function $\mathbf{W} \in L^2(\Lambda; \mathbb{C}^{2 \times 2})$, and where δ is some "perturbative" real parameter which will be specified hereafter. In the case of non-perturbed/structured photonic graphene $(\delta = 0)$, the lattice possesses several symmetries and we then denote the material weight by $\mathbf{W} = \mathbf{A}$, where $\mathbf{A} \in L^2(\Lambda; \mathbb{C}^{2 \times 2})$ is Hermitian, positive definite, and uniformly elliptic. The non-perturbated material satisfies the \mathcal{CRP} -invariance: $\overline{\mathbf{A}}(-\mathbf{x}) = \mathbf{A}(\mathbf{x})$, $\mathbf{A}(\mathbf{R}^*\mathbf{x}) = \mathbf{R}^*\mathbf{A}(\mathbf{x})\mathbf{R}$ and $\mathbf{A}(\mathbf{x} + \mathbf{v}) = \mathbf{A}(\mathbf{x})$, for $\mathbf{v} \in \Lambda$ and where the rotation matrix \mathbf{R} is defined by

$$\mathbf{R} = \frac{1}{2} \begin{pmatrix} -1 & \sqrt{3} \\ -\sqrt{3} & -1 \end{pmatrix}.$$

Hereafter, we will choose $\mathbf{A}(\mathbf{x}) = a(\mathbf{x})\mathbf{I}_{2\times 2}$. Practically, \mathbf{A} , \mathbf{W} will be assumed continuously differentiable. We refer to [19,22] for some more detailed properties. Notice that the *Fermi velocity* is defined from the first eigenfunction of $\mathcal{L}^0(\delta = 0)$, where

$$\mathcal{L}^0 = -\nabla a(\mathbf{x}) \cdot \nabla - a(\mathbf{x}) \triangle$$
.

The electromagnetic wave dynamics in that case is hence modeled by

$$i\partial_t \psi = a(\mathbf{x}) \triangle \psi + \nabla a(\mathbf{x}) \cdot \nabla \psi.$$

Unlike the computation of the edge-states which may require a transformation of the operator under consideration (for instance due to dissolution in continuum [14] or spectral pollution [18]), the computation of the time-dependent solution can be "directly" performed.

1.1. Perturbed photonic graphene

In the case of perturbed photonic graphene ($\delta \neq 0$), we rewrite

$$W(x) := A(x) + M(x),$$

where $\mathbf{x} = (x, y)$, and \mathbf{M} models to a \mathcal{PC} -symmetry breaking. We again refer to [22] for details. Let us recall that the edge states are the eigenfunctions associated to the point spectrum of the following eigenvalue problem, for $k_{\parallel} \in [0, 2\pi)$:

$$\begin{cases} \mathcal{L}^{\delta} \psi_e^{\delta}(\mathbf{x}; k_{\parallel}) = E_e^{\delta}(k_{\parallel}) \psi_e^{\delta}(\mathbf{x}; k_{\parallel}), \\ \psi_e^{\delta}(\mathbf{x} + \mathbf{v}_1; k_{\parallel}) = e^{\mathrm{i}k_{\parallel}} \psi_e^{\delta}(\mathbf{x}; k_{\parallel}), \\ \psi_e^{\delta}(\mathbf{x}; k_{\parallel}) \rightarrow 0 \quad \text{as} \quad |\mathbf{x} \cdot \mathbf{k}_2| \rightarrow +\infty, \end{cases}$$

where ψ_e^{δ} is a so-called edge state and E_e^{δ} the corresponding energy. In this paper, we will be particularly interested in \mathcal{PC} -symmetry breaking, thanks to the wall function η having a shape determined by a *smooth* function \mathbf{F} , the *wall-shape* function. We assume hereafter that $\mathbf{F}(\mathbf{0}) = \mathbf{0}$, and that η is a smooth function, such that

$$\eta'(0) = 1, \quad \eta(x) \sim x \quad \text{as} \quad x \to 0,$$

 $\eta(x) \to \pm 1, \quad \eta'(x) \to \pm 0 \quad \text{as} \quad x \to \pm \infty.$ (2)

Following [18], we will take $\eta(x) = \tanh(x)$. For the \mathcal{P} -symmetry breaking case, we then consider

$$\mathbf{W}(\mathbf{x}) := a(\mathbf{x})\mathbf{I}_{2\times 2} + \delta\eta(\mathbf{k}_2 \cdot \mathbf{F}(\mathbf{x}))b(\mathbf{x})\mathbf{I}_{2\times 2}, \tag{3}$$

and for the C-symmetry breaking

$$\mathbf{W}(\mathbf{x}) := a(\mathbf{x})\mathbf{I}_{2\times 2} + \delta\eta(\mathbf{k}_2 \cdot \mathbf{F}(\mathbf{x}))b(\mathbf{x})\sigma, \tag{4}$$

where σ the following Pauli matrix

$$\sigma = \begin{pmatrix} 0 & -i \\ i & 0 \end{pmatrix}$$
.

Let us recall that k_2 is orthogonal to v_1 . We then propose to apply a Bloch transformation of the operator, which allows us to simplify the analysis and approximation of the Schrödinger operator. Setting

$$\psi_e^{\delta}(\mathbf{x}, k_{\parallel}) = \exp\left(i\frac{k_{\parallel}}{2\pi}\mathbf{k}_1 \cdot \mathbf{x}\right)\phi_e^{\delta}(\mathbf{x}, k_{\parallel}),$$

we easily see that ϕ_e^{δ} satisfies the following system

$$\begin{cases} \mathcal{S}^{\delta} \phi_e^{\delta}(\mathbf{x}; k_{\parallel}) = E_e^{\delta}(k_{\parallel}) \phi_e^{\delta}(\mathbf{x}; k_{\parallel}), \\ \phi_e^{\delta}(\mathbf{x} + \mathbf{v}_1; k_{\parallel}) = \phi_e^{\delta}(\mathbf{x}; k_{\parallel}), \\ \phi_e^{\delta}(\mathbf{x}; k_{\parallel}) \rightarrow 0, \quad \text{as} \quad |\mathbf{x} \cdot \mathbf{k}_2| \rightarrow +\infty, \end{cases}$$

where we have denoted

$$S^{\delta} = -\left(\nabla + i\frac{k_{\parallel}}{2\pi}\mathbf{k}_{1}\right) \cdot \mathbf{W}(\mathbf{x})\left(\nabla + i\frac{k_{\parallel}}{2\pi}\mathbf{k}_{1}\right).$$

We next denote by ψ_{k_\parallel} the solution to the following time-dependent Schrödinger equation

$$\begin{cases}
i \partial_{t} \psi_{k_{\parallel}}(\mathbf{x}, t) = \mathcal{S}^{\delta} \psi_{k_{\parallel}}(\mathbf{x}, t), \text{ on } \Omega \times (0, T), \\
\psi_{k_{\parallel}}^{\delta}(\mathbf{x}, 0) = \phi_{e}^{\delta}(\mathbf{x}; k_{\parallel}), \text{ on } \Omega, \\
\psi_{k_{\parallel}}^{\delta}(\mathbf{x} + \mathbf{v}_{1}, t) = \psi_{k_{\parallel}}^{\delta}(\mathbf{x}, t), \text{ on } \Omega \times (0, T), \\
\psi_{k_{\parallel}}^{\delta}(\mathbf{x}, t) \to 0, \text{ as } |\mathbf{x} \cdot \mathbf{k}_{2}| \to +\infty.
\end{cases}$$
(5)

In particular, when $\mathbf{W} = \mathbf{A} + \mathbf{M}$ with $\mathbf{A}(\mathbf{x}) = a(\mathbf{x})\mathbf{I}_{2\times 2}$ and $\mathbf{M}(\mathbf{x}) = \delta\eta (\mathbf{k}_2 \cdot \mathbf{F}(\mathbf{x}))b(\mathbf{x})\sigma$ (resp. $\mathbf{M}(\mathbf{x}) = \delta\eta (\mathbf{k}_2 \cdot \mathbf{F}(\mathbf{x}))b(\mathbf{x})\mathbf{I}_2$) for \mathcal{C} -symmetry (resp. \mathcal{P} -symmetry) breaking, we get

$$S^{\delta} = -\nabla \cdot (\mathbf{A} + \mathbf{M})\nabla + \frac{k_{\parallel}^{2}}{4\pi^{2}}\mathbf{k}_{1} \cdot (\mathbf{A}(\mathbf{x}) + \mathbf{M}(\mathbf{x}))\mathbf{k}_{1}$$
$$-i\left(\frac{k_{\parallel}}{2\pi}\nabla \cdot (\mathbf{A}(\mathbf{x}) + \mathbf{M}(\mathbf{x}))\mathbf{k}_{1} + \frac{k_{\parallel}}{2\pi}\mathbf{k}_{1} \cdot (\mathbf{A}(\mathbf{x}) + \mathbf{M}(\mathbf{x}))\nabla\right).$$

Notice that as the function a is real, the dynamical equation contains in particular a transport and a reaction term. Moreover when \mathbf{M} is null the spectrum of \mathcal{S}^0 is discrete $E_1(\mathbf{k}) \leqslant \cdots \leqslant E_n(\mathbf{k}) \leqslant \cdots$ for \mathbf{k} in the first Brillouin zone, and the corresponding eigenvalues are such that $\Phi(\mathbf{x} + \mathbf{v}) = e^{i\mathbf{k}\cdot\mathbf{v}}\Phi(\mathbf{x})$, for all $\mathbf{v} \in \Lambda$; see [22].

1.2. Examples of material functions

As an illustration of the above introduction, we propose in this paragraph to report the graph of some functions modeling different materials under consideration in this paper. Let us set

$$w(\mathbf{x}) := a(\mathbf{x}) + m(\mathbf{x}),$$

where

$$a(\mathbf{x}) = \alpha + \beta \sum_{i=1}^{3} \cos(\mathbf{k}_{i} \cdot \mathbf{x}), \ m(\mathbf{x}) = \delta \eta (\delta \mathbf{k}_{2} \cdot \mathbf{F}(\mathbf{x})) \sum_{i=1}^{3} \sin(\mathbf{k}_{i} \cdot \mathbf{x}),$$
 (6)

where the wall function is given by $\eta = \tanh$ and with the following constants: $\delta = 1$, $\alpha = 0.3$, $\beta = 0.1$, and where $F(\mathbf{x})$ is the wall-shape function. We report the graph of a, $a_x (= \partial_x a)$ and $a_y (= \partial_y a)$ in Fig. 1.

In Fig. 2 (Top)(resp. 2 (Bottom)), we report for $\mathbf{F}(\mathbf{x}) = (x, y)^T$ (resp. $\mathbf{F}(\mathbf{x}) = (x, y/2 + \sin(y)/2)^T$) the graphes of w, w_x , and w_y , illustrating the effect of the wall perturbation on the material structure.

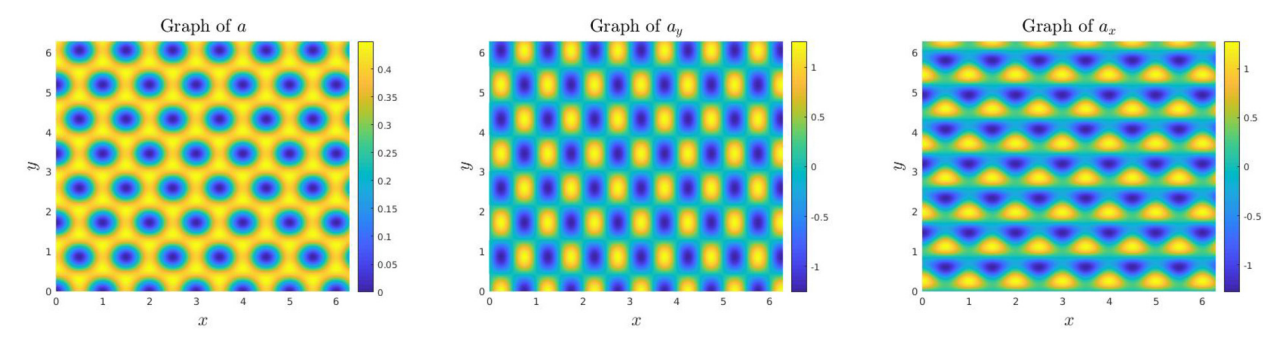


Fig. 1. Graph of a, a_x and a_y . (For interpretation of the colors in the figure(s), the reader is referred to the web version of this article.)

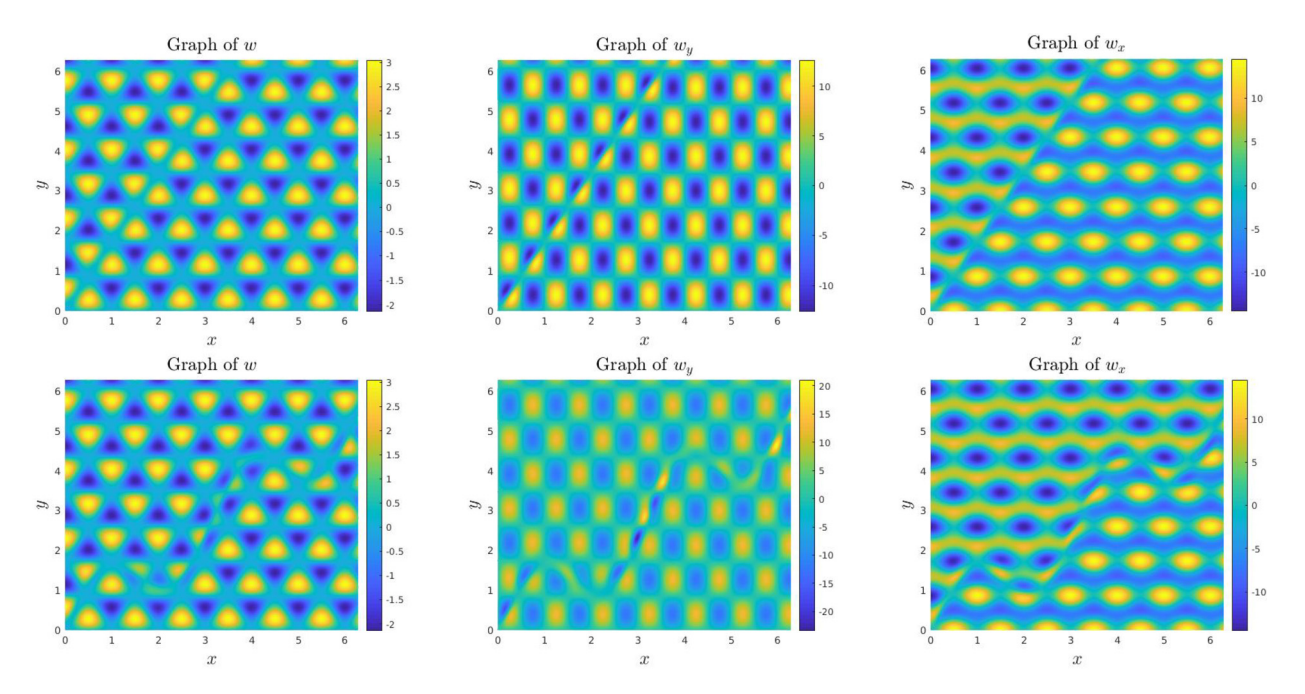


Fig. 2. Graph of w, w_x and w_y . (Top) $F(x, y) = (x, y)^T$. (Bottom) $F(x, y) = (x + y/2 + \sin(y/2))^T$.

1.3. Choice of the computational method

The mathematical model under consideration is a two-dimensional (2D) time-dependent Schrödinger equation with non-constant coefficients; and which are periodic in the direction v_1 . Due to this periodicity it is natural to use a Fourier-based method. The chosen method is an IMEX pseudospectral method based on the pseudodifferential representation of the Schrödinger Hamiltonian, which was originally developed in [2,5]. Alternatively, a higher order finite element methods could have been used in order to benefit from the variational structure of the equation. However, considering the complexity of the equation, the simple pseudospectral method allowing for approximating PDE with non-constant coefficients, is here preferred. Let us mention that among several existing techniques for approximating the Schrödinger equation under consideration, numerical techniques such as Generalized Finite Difference Methods which can easily be coupled with PML, allow for a large flexibility and simplicity of implementation while keeping a good accuracy and nice mathematical properties [10,28].

In this paper, we are in particular interested in edge states, which are eigenstates to the Schrödinger operator. The latter are known [22] to be local in the direction \mathbf{k}_2 , which is orthogonal to \mathbf{v}_1 . Moreover, as the solution is not periodic in that direction, it is then necessary to avoid the periodicity naturally induced by the Fourier transform. In this goal, we propose to combine our pseudospectral method with perfectly matched layers [11] in the direction \mathbf{k}_2 . Interestingly, this combination does not complexify the structure of the overall algorithm. Some mathematical and numerical properties of the derived algorithm will be proposed in Section 3.

1.4. Organization of the paper

This paper is organized as follows. In Section 2, we discuss some mathematical properties of the proposed model in particular regarding the dynamics of the wavefunction in the neighborhood of the wall. Section 3 is dedicated to the derivation and properties of a computational pseudospectral method for solving the time-dependent Schrödinger equation under consideration. In Section 4, we present several numerical experiments illustrating the properties of the derived method and simulating some physical phenomena. We conclude in Section 5.

2. Some mathematical properties

In this section, we present some simple but important mathematical properties of the studied model, in particular, regarding the evolution of the wavefunctions in the neighborhood of the wall.

2.1. Basic information

Due to the complexity of the equation, the analysis of the wavefunction dynamics and possible capture of edge states by the wall, may require to work on a simplified model. In this goal, we will derive below equivalent equations in the case of symmetry-breaking. For the sake of simplicity, we will consider infinite spatial domain \mathbb{R}^2 , which is a reasonable assumption, since we will mainly be interested in localized solutions. In particular, we assume that the initial condition has compact support in the space domain. From

$$i\partial_{t}\psi = -\nabla \cdot (\boldsymbol{W}(\boldsymbol{x})\nabla),$$

we multiply by $\overline{\psi} \in L^2(\mathbb{R}^2)$ leading to

$$\frac{1}{2}\frac{d}{dt}\|\psi\|_2^2 = -\operatorname{Im}\int \boldsymbol{W}(\boldsymbol{x})|\nabla\psi(\boldsymbol{x},t)|^2d\boldsymbol{x}.$$

P-symmetry breaking. In this case,

$$\mathbf{W}(\mathbf{x}) := a(\mathbf{x})\mathbf{I}_{2\times 2} + \delta\eta(\mathbf{k}_2 \cdot \mathbf{F}(\mathbf{x}))b(\mathbf{x})\mathbf{I}_{2\times 2}$$
.

Hence as W is real, the L^2 -norm of the wavefunction ψ is trivially conserved. Interestingly, we also get the following identity

$$\operatorname{Im} \int \overline{\psi} \psi_t d\mathbf{x} = \int a(\mathbf{x}) |\psi(\mathbf{x}, t)|^2 + \delta \eta \big(\mathbf{k}_2 \cdot \mathbf{F}(\mathbf{x}) \big) b(\mathbf{x}) |\nabla \psi(\mathbf{x}, t)|^2 d\mathbf{x}.$$

C-symmetry breaking. In this case,

$$\mathbf{W}(\mathbf{x}) := a(\mathbf{x})\mathbf{I}_{2\times 2} + \delta\eta(\mathbf{k}_2 \cdot \mathbf{F}(\mathbf{x})b(\mathbf{x}))\boldsymbol{\sigma}$$

and the L^2 -norm conservation also holds. Indeed

$$\frac{1}{2}\frac{d}{dt}\|\psi\|_2^2 = \operatorname{Re} \int b(\mathbf{x})\boldsymbol{\gamma} \nabla \psi(\mathbf{x}) \cdot \nabla \overline{\psi}(\mathbf{x}) d\mathbf{x} = 0.$$

where

$$\gamma = \begin{pmatrix} 0 & 1 \\ -1 & 0 \end{pmatrix}.$$

2.2. Equivalent equation in symmetry breaking

Let us discuss the equivalent equation in the case of symmetry breaking. More specifically, we are interested in the equivalent equation close and away from the wall.

C-symmetry breaking. We first discuss the dynamics along the wall in the case of C-symmetry breaking. We assume that the Bloch transform has not been applied yet, i.e. we consider Equation (1)

$$\mathrm{i}\,\partial_t\psi = -\nabla\cdot(\boldsymbol{W}(\boldsymbol{x})\cdot\nabla)\psi\,,$$

where $\mathbf{W} = a\mathbf{I}_{2\times 2} + m\boldsymbol{\sigma}$ and with

$$m(\mathbf{x}) = \delta \eta (\delta \mathbf{k}_2 \cdot \mathbf{F}(\mathbf{x})) b(\mathbf{x})$$
.

Notice first that

$$\mathbf{W}(\mathbf{x})\nabla\cdot\nabla = a(\mathbf{x}) + m(\mathbf{x})\boldsymbol{\sigma}\nabla\cdot\nabla = a(\mathbf{x})\Delta$$
.

as $\sigma \nabla \cdot \nabla = \mathbf{0}$. Next

$$\nabla \boldsymbol{W}(\boldsymbol{x}) \cdot \nabla = \nabla a(\boldsymbol{x}) + \nabla m(\boldsymbol{x}) \boldsymbol{\sigma} \cdot \nabla$$

= $\nabla a(\boldsymbol{x}) + \nabla m(\boldsymbol{x}) \cdot (-i \partial_{\nu}, i \partial_{\nu})^{T}$.

Denoting $\mathbf{F} = (F_x, F_y)^T$ we then get

$$\nabla \boldsymbol{W}(\boldsymbol{x}) \cdot \nabla = \nabla a(\boldsymbol{x}) + \delta \eta (\delta \boldsymbol{k}_2 \cdot \boldsymbol{x}) \nabla b(\boldsymbol{x}) \cdot (-i \partial_y, i \partial_x)^T$$

= $\delta^2 b(\boldsymbol{x}) \eta' (\delta \boldsymbol{k}_2 \cdot \boldsymbol{F}(\boldsymbol{x})) \boldsymbol{k}_2 \cdot (\partial_x F_x(\boldsymbol{x}), \partial_y F_y(\boldsymbol{x})) \cdot (-i \partial_y, i \partial_x)^T$.

Then

$$\nabla \boldsymbol{W}(\boldsymbol{x}) \cdot \nabla = \nabla a(\boldsymbol{x}) + i K_{x}(\boldsymbol{x}) \partial_{x} + i K_{y}(\boldsymbol{x}) \partial_{y} + i L_{x}(\boldsymbol{x}) \partial_{x} + i L_{y}(\boldsymbol{x}) \partial_{y},$$

where

$$K_{\mathbf{x}}(\mathbf{x}) = -\delta^2 b(\mathbf{x}) \eta' (\delta \mathbf{k}_2 \cdot \mathbf{F}(\mathbf{x})) k_2^{\mathbf{y}} (\partial_{\mathbf{y}} F_{\mathbf{y}}(\mathbf{x}), K_{\mathbf{y}}(\mathbf{x}) = \delta^2 b(\mathbf{x}) \eta' (\delta \mathbf{k}_2 \cdot \mathbf{F}(\mathbf{x})) k_2^{\mathbf{y}} (\partial_{\mathbf{x}} F_{\mathbf{x}}(\mathbf{x}),$$

and

$$L_{X}(\mathbf{x}) = -\delta \eta \left(\delta \mathbf{k}_{2} \cdot \mathbf{F}(\mathbf{x}) \right) \partial_{y} b(\mathbf{x}),$$

$$L_{Y}(\mathbf{x}) = \delta \eta \left(\delta \mathbf{k}_{2} \cdot \mathbf{F}(\mathbf{x}) \right) \partial_{x} b(\mathbf{x}).$$

Denoting the vector fields $\mathbf{K} = (K_x, K_y)^T$ and $\mathbf{L} = (L_x, L_y)^T$, the equation then reads

$$\partial_t \psi = i(a(\mathbf{x}) + m(\mathbf{x})) \triangle \psi + i \nabla a(\mathbf{x}) \cdot \nabla \psi + \mathbf{K}(\mathbf{x}) \cdot \nabla \psi + \mathbf{L}(\mathbf{x}) \cdot \nabla \psi. \tag{7}$$

We now analyze the contribution of this velocity fields K, L close and away from the wall.

Close to the wall. Thanks to the assumption (2), close to the wall we have $\eta(x) \sim x$ and $\eta' \sim 1$. More specifically, denoting by \mathcal{N}_W a neighborhood of the wall defined as

$$\mathcal{N}_W = \left\{ \mathbf{x} / \mathbf{k}_2 \cdot \mathbf{F}(\mathbf{x}) = o(1) \right\},\tag{8}$$

where o(1) refers to $\delta \to 0$. In particular, we have, for $\mathbf{x} \in \mathcal{N}_W$,

$$\eta(\mathbf{k}_2 \cdot \mathbf{F}(\mathbf{x})) \sim_{\mathbf{x} \in \mathcal{N}_W} \mathbf{k}_2 \cdot \mathbf{F}(\mathbf{x}) = o(1). \tag{9}$$

Hence

$$\begin{split} K_{X}(\boldsymbol{x}) \sim_{\boldsymbol{x} \in \mathcal{N}_{W}} -\delta^{2}b(\boldsymbol{x})k_{2}^{y}\partial_{y}F_{y}(\boldsymbol{x}), \\ K_{y}(\boldsymbol{x}) \sim_{\boldsymbol{x} \in \mathcal{N}_{W}} \delta^{2}b(\boldsymbol{x})k_{2}^{x}\partial_{x}F_{x}(\boldsymbol{x}), \end{split}$$

and

$$L_{X}(\mathbf{x}) \sim_{\mathbf{x} \in \mathcal{N}_{W}} -\delta^{2} \mathbf{k}_{2} \cdot \mathbf{F}(\mathbf{x}) \partial_{x} b(\mathbf{x}) = \delta \partial_{x} b(\mathbf{x}) o(\delta),$$

$$L_{Y}(\mathbf{x}) \sim_{\mathbf{x} \in \mathcal{N}_{W}} \delta^{2} \mathbf{k}_{2} \cdot \mathbf{F}(\mathbf{x}) \partial_{y} b(\mathbf{x}) = \delta \partial_{y} b(\mathbf{x}) o(\delta).$$

In other words, close to the wall the transport is mainly driven by the vector field K (as L is negligible compared to K). More specifically, we observe that, close to the wall, the direction of the propagation is given by the following velocity field:

$$\mathbf{V}(\mathbf{x}) = \delta^2 b(\mathbf{x}) \left(-k_2^y \partial_y F_y(\mathbf{x}), k_2^x \partial_x F_x(\mathbf{x}) \right)^T,$$

where $\mathbf{F}(\mathbf{x}) = (x, f(y))^T$, we get

$$\mathbf{V}(\mathbf{x}) = \delta^2 b(\mathbf{x}) \mathbf{k}_2 \cdot (-f'(\mathbf{y}), 1)^T$$
.

Regarding m, we also have in the neighborhood of the wall:

$$m(\mathbf{x}) \sim_{\mathbf{x} \in \mathcal{N}_W} \delta b(\mathbf{x}) o(\delta)$$
.

Based on the above discussion, the model behaves as follows.

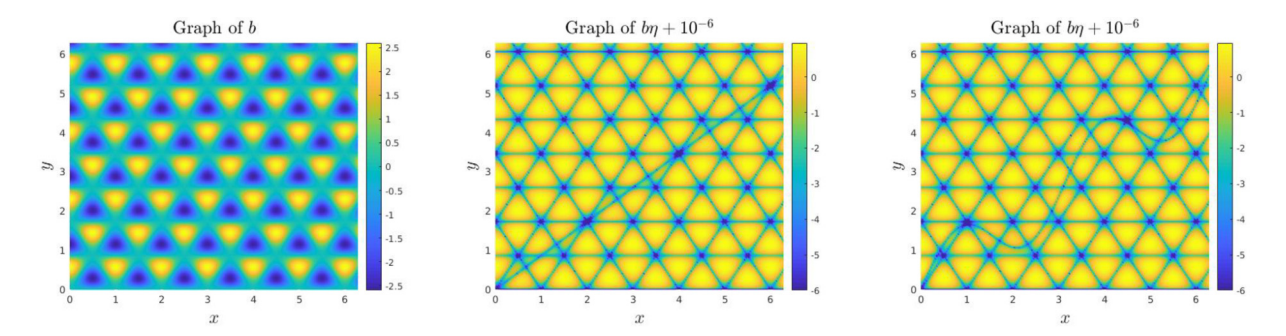


Fig. 3. (Left) Graph of *b* in logscale. (Middle) Graph of $b\eta + 10^{-6}$ for $\mathbf{F}(\mathbf{x}) = (x, y/2)^T$ (Right) Graph of $b\eta + 10^{-6}$ for $\mathbf{F}(\mathbf{x}) = (x, y/2 + \sin(2y)/2)^T$.

Definition 2.1. The *equivalent equation* to (7) close to the wall in the case of C-symmetry is defined as:

$$\partial_t \psi = i \left(a(\mathbf{x}) + \delta b(\mathbf{x}) o(\delta) \right) \triangle \psi + i \nabla a(\mathbf{x}) \cdot \nabla \psi + \mathbf{V}(\mathbf{x}) \cdot \nabla \psi . \tag{10}$$

The initial and boundary conditions are the same as in (5).

We make several important remarks as below.

- There is in general, no guarantee that *m* is negligible compared to *a*, so that we keep its contribution in the equivalent equation.
- The amplitude of the propagation velocity is mainly given by the term $\delta^2 b(\mathbf{x})$. As b is an oscillatory function, we then expect a non-constant velocity, which can essentially vanish when b is null (or practically close to 0). Considering $b(\mathbf{x}) = \sum_{i=1}^{3} \cos(\mathbf{k}_i \cdot \mathbf{x})$ (or sin), and we denote

$$C_b := \left\{ \mathbf{x} \in \Lambda / b(\mathbf{x}) = 0 \right\}. \tag{11}$$

In this case C_b is the union $\bigcup_k C_k$ of circles C_k where some of these circles are truncated by the boundary of Λ . In this case, we observe that the vector field V is null (in fact even L would be null in this case). We now denote

$$W := \left\{ \boldsymbol{x} \in \Lambda / \boldsymbol{k}_2 \cdot \boldsymbol{F}(\boldsymbol{x}) = 0 \right\}.$$

At the intersection of C_b and W, the wavefunction will no more be driven by V. See Fig. 4, where the wall is identified as a curved line crossing some circles C_k .

- On C_b , notice that m in (10) will also be null. That is the kinetic contribution along the wall also vanishes on C_b .
- If a is small, the wavefunction (including edge states) with initial position inside a disc \mathcal{D}_k with boundary \mathcal{C}_k , will be trapped inside \mathcal{D}_k .

Away from the wall. In this case, we define

$$\mathcal{N}_a := \{ \boldsymbol{x} / \eta(\delta \boldsymbol{k}_2 \cdot \boldsymbol{F}(\boldsymbol{x})) | = 1 - o(\delta) \},$$

with this time, $\eta'(\mathbf{x}) \sim_{\mathbf{x} \in \mathcal{N}_a} 0$, so that $K_{\mathbf{x}}(\mathbf{x}) \sim_{\mathbf{x} \in \mathcal{N}_a} 0$ and $K_{\mathbf{y}}(\mathbf{x}) \sim_{\mathbf{x} \in \mathcal{N}_a} 0$. Away from the wall, \mathbf{L} is no more negligible, and $m(\mathbf{x}) \sim_{\mathbf{x} \in \mathcal{N}_a} \pm 1$. Hence, the equivalent equation can be defined as follows.

Definition 2.2. The *equivalent equation* to (7) far from the wall in the C-symmetry case is defined as:

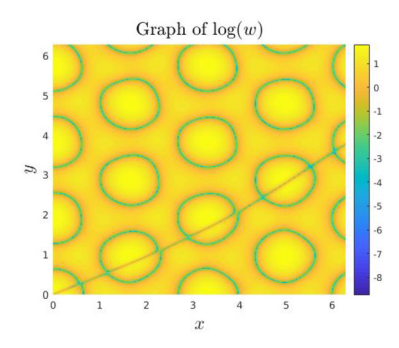
$$\partial_t \psi = i \left(a(\mathbf{x}) + \delta b(\mathbf{x}) \operatorname{sgn}(\mathbf{k}_2 \cdot \mathbf{x}) \right) \triangle \psi - i \nabla a(\mathbf{x}) \cdot \nabla \psi + \mathbf{L}(\mathbf{x}) \cdot \nabla \psi , \tag{12}$$

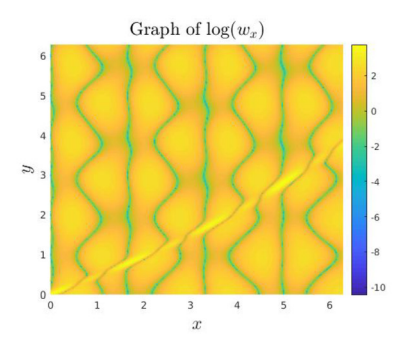
where sgn is the sign function. The initial and boundary conditions are the same as in (5).

In this paper, b will be typically taken as $b: \mathbf{x} \mapsto \sum_{i=1}^3 \cos(\mathbf{k}_i \cdot \mathbf{x})$ (or \sin) where $\mathbf{k}_1 = 2\pi (1, \sqrt{3})^T/\sqrt{3}$, $\mathbf{k}_2 = 2\pi (1, -\sqrt{3})^T/\sqrt{3}$ and $\mathbf{k}_3 = -\mathbf{k}_1 - \mathbf{k}_2$. Let us report the graph of b over the domain $[0, 2\pi]^2$ in Fig. 3 (Left) and in Fig. 3 (Middle), (resp. (Right)) the graph of $\mathbf{x} \mapsto \log \left(10^{-6} + \tanh(\delta \mathbf{k}_2 \cdot \mathbf{F}(\mathbf{x})) \sum_{i=1}^3 \sin(\mathbf{k}_i \cdot \mathbf{x})\right)$ for $\delta = 1$ and $\mathbf{F}(\mathbf{x}) = (x, y/2)^T$ (resp. $\mathbf{F}(\mathbf{x}) = (x, y/2 + \sin(2y)/2)^T$). We have added the coefficient 10^{-6} to better visualize the zone where the vector field \mathbf{V} vanishes (or is small). As expected, along the wall the velocity field actually vanishes. These zones correspond to the intersection to the wall function \mathbf{F} with the zeros of b.

In Fig. 4, we report the graph in logscale of w := a + m and w_x , w_y , illustrating the intersection point of C_b and W for

$$a(\mathbf{x}) = 0.1 \sum_{i=1} \sin(\mathbf{k}_i \cdot \mathbf{x}), \ m(\mathbf{x}) = \delta \tanh(\delta(\mathbf{k}_2 \cdot \mathbf{F}(\mathbf{x}))) \sum_{i=1} \sin(0.5\mathbf{k}_i \cdot \mathbf{x}),$$





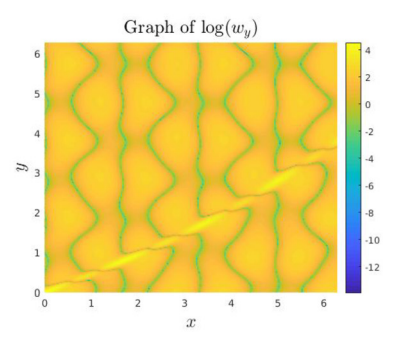


Fig. 4. Graph of $\log |w|$, $\log |w_x|$ and $\log |w_y|$.

and $\delta = 2$ and $\mathbf{F}(\mathbf{x}) = (x, 0.25 \sin(y))^T$. The use of the logscale allows to more clearly identify C_b (union of circles) as well as the domain W. The claim is that, in the \mathcal{C} -symmetry case, at the intersection points between C_b and W a wavefunction would stop propagating. More generally, the wavefunction will be trapped inside the disc of contour C_k , as we will numerically observe in Section 4.

 \mathcal{P} -symmetry breaking. A similar discussion is proposed in the case of \mathcal{P} -symmetry breaking.

Close to the wall. In the neighborhood of the wall, that is in \mathcal{N}_W the equivalent equation reads as follows.

Definition 2.3. The *equivalent equation* to (7) close to the wall in the \mathcal{P} -symmetry case is defined as:

$$\partial_t \psi = i \left(a(\mathbf{x}) + \delta b(\mathbf{x}) o(\delta) \right) \Delta \psi + i \nabla a(\mathbf{x}) \cdot \nabla \psi + i \mathbf{Z}(\mathbf{x}) \cdot \nabla \psi , \tag{13}$$

where

$$\mathbf{Z}(\mathbf{x}) = \delta^2 b(\mathbf{x}) \left(k_2^{\mathsf{x}} \partial_{\mathsf{y}} F_{\mathsf{y}}(\mathbf{x}), k_2^{\mathsf{y}} \partial_{\mathsf{y}} F_{\mathsf{y}}(\mathbf{x}) \right)^T.$$

The initial and boundary conditions are the same as in (5).

Interestingly in this case the wall does not make appear a transport term, but a "coupling" term instead.

Away from the wall. Away from the wall, that in the set \mathcal{N}_a , we define:

Definition 2.4. The equivalent equation to (7) far to the wall in the \mathcal{P} -symmetry case is defined as:

$$\partial_t \psi = i \left(a(\mathbf{x}) + \delta b(\mathbf{x}) \operatorname{sgn}(\mathbf{k}_2 \cdot \mathbf{x}) \right) \triangle \psi + i \nabla a(\mathbf{x}) \cdot \nabla \psi + \delta \eta (\delta \mathbf{k}_2 \cdot \mathbf{x}) \nabla b(\mathbf{x}) \cdot \nabla \psi , \tag{14}$$

where sgn is the sign function. The initial and boundary conditions are the same as in (5).

3. PML-based pseudospectral computational method

In this section, we derive a pseudospectral method which naturally imposes periodic boundary conditions. As periodicity is only necessary in the direction v_1 , PML will be introduced for absorbing the wavefunction in the direction v_1^{\perp} .

We first describe the spatial discretization of the Schrödinger equation under consideration. For efficiency reasons and as the solution is periodic only in the direction k_2 , it is natural to use a Fourier-based method for solving the Schrödinger equation. However, as the coefficients of the equation are non-constant, and as we need to impose Dirichlet or radiative conditions it is also necessary to design a computational method that could take these constraints into account. The method we propose is a pseudospectral method allowing i) to easily take into account non-constant coefficients, and ii) a natural combination with Perfectly Matched Layers in order to address the null Dirichlet boundary conditions (or radiative conditions) in the direction $\mathbf{v}_{\perp}^{\perp}$. We refer to [2,5] for details about the proposed approach in the framework for quantum physics.

3.1. Pseudospectral method

The proposed computational method was used in different frameworks, linear and nonlinear Schrödinger equations [5,7], Dirac equations [1,2,8] or fractional PDE [3]. Throughout this section, we assume that the equation is solved on a generic truncated domain $[-L_1, L_1] \times [-L_2, L_2] \subsetneq \mathbb{R}^2$. We define two sets of grid-points in real and Fourier spaces labeled by the multi-indices $\mathbf{k} = (k_1, k_2)$ and $\mathbf{p} = (p_1, p_2)$:

$$\begin{split} \mathcal{D}_{N}^{(x)} &= \left\{ \boldsymbol{x_{k}} := \boldsymbol{x_{k_{1},k_{2}}} = (x_{k_{1}}^{1}, x_{k_{2}}^{2}) \right\}_{\boldsymbol{k} \in \mathcal{O}_{N}^{(x)}}, \\ \mathcal{D}_{N}^{(\xi)} &= \left\{ \boldsymbol{\xi_{p}} := \boldsymbol{\xi_{p_{1},p_{2}}} = (\xi_{p_{1}}^{1}, \xi_{p_{2}}^{2}) \right\}_{\boldsymbol{p} \in \mathcal{O}_{N}^{(\xi)}}, \end{split}$$

where $N := (N_1, N_2)$, with $N_i \in 2\mathbb{N}^*$ the number of points in each dimension, and with

$$\mathcal{O}_N^{(x)} = \left\{ \boldsymbol{k} \in \mathbb{N}^2 / (k_i = 0, \dots, N_i - 1)_{i=1,2} \right\},$$

$$\mathcal{O}_N^{(\xi)} = \left\{ \boldsymbol{p} \in \mathbb{N}^2 / \left(p_i = -\frac{N_i}{2}, \dots, \frac{N_i}{2} - 1 \right)_{i=1,2} \right\}.$$

The set $\mathcal{D}_N^{(x)}$ defines a mesh with equidistant positions in each dimension with sizes (for i=1,2)

$$x_{k_{i+1}}^{i} - x_{k_{i}}^{i} = h_{i} = 2L_{i}/N_{i}$$
.

One can deduce that the discrete wavenumbers in Fourier space are given by (for $i = 1, \dots, D$)

$$\xi_{n_i}^i = p_i \pi / L_i$$
.

The wavefunction $\psi(\mathbf{x},t)$ is discretized spatially by a projection onto the spatial mesh while $\widetilde{\psi}$ denotes the wavefunction in Fourier space. We denote by $\psi_{\mathbf{k}}^n$ the approximate wavefunction at time t_n and position $\mathbf{x}_{\mathbf{k}}$, and by $\widetilde{\psi}_{\mathbf{p}}^n$ the wavefunction in momentum (Fourier) space at time t_n and momentum $\boldsymbol{\xi}_{\mathbf{p}}$. The discrete wavefunctions $\psi_{\mathbf{k}}^n$ and $\widetilde{\psi}_{\mathbf{p}}^n$ are related by the discrete Fourier transform pair:

$$\begin{split} \widetilde{\boldsymbol{\psi}}_{\pmb{p}}^n &= \mathcal{F}(\boldsymbol{\psi}_{\pmb{k}}^n) := \sum_{k=0}^{N-1} \boldsymbol{\psi}_{\pmb{k}}^n e^{-\mathrm{i}\boldsymbol{\xi}_{\pmb{p}}\cdot(\pmb{x}_{\pmb{k}}+\pmb{L})}, \\ \widehat{\boldsymbol{\psi}}_{\pmb{k}}^n &= \mathcal{F}^{-1}(\widetilde{\boldsymbol{\psi}}_{\pmb{p}}^n) := \frac{1}{N} \sum_{n=-N/2}^{N/2-1} \widetilde{\boldsymbol{\psi}}_{\pmb{p}}^n e^{\mathrm{i}\boldsymbol{\xi}_{\pmb{p}}\cdot(\pmb{x}_{\pmb{k}}+\pmb{L})}, \end{split}$$

where $\mathbf{L} = (L_1, L_2)$. We also define the partial discrete Fourier coefficients in each dimension as:

$$\begin{split} \widetilde{\psi}^n_{\boldsymbol{k}|k_i \to p_i} &= \mathcal{F}_i(\psi^n_{\boldsymbol{k}}) := \sum_{k_i = 0}^{N_i - 1} \psi^n_{\boldsymbol{k}} e^{-\mathrm{i} \xi^i_{p_i}(x^i_{k_i} + L_i)}, \\ \widehat{\psi}^n_{\boldsymbol{k}} &= \mathcal{F}_i^{-1}(\widetilde{\psi}^n_{\boldsymbol{k}}) := \frac{1}{N_i} \sum_{n_i = -N_i/2}^{N_i/2 - 1} \widetilde{\psi}^n_{\boldsymbol{k}|k_i \to p_i} e^{\mathrm{i} \xi^i_{p_i}(x^i_{k_i} + L_i)}, \end{split}$$

where the notation $\mathbf{k}|k_i \to p_i$ means that the index k_i in the set \mathbf{k} is replaced by the index p_i and where the partial DFT operator in the ith coordinate is denoted by $\mathcal{F}_i(\cdot)$. In practice, all of these Fourier transforms are performed using the Fast Fourier Transform (FFT). In order to approximate the partial derivative, we use pseudospectral approximations of the pseudodifferential representation of the derivative operators. That is, we introduce the pseudodifferential operator $[[\partial_i]]$ defined as follows

$$\partial_{i}\psi(\mathbf{x}_{k},t_{n}) \approx \left\{ [[\partial_{i}]]\psi^{n}\right\}_{k} := \frac{1}{N_{i}} \sum_{p_{i}=-N_{i}/2}^{N_{i}/2-1} i\xi_{p_{i}}^{i} \widetilde{\psi}_{\mathbf{k}|k_{i}\to p_{i}}^{n} e^{i\xi_{p_{i}}^{i}(x_{k_{i}}^{i}+L_{i})}, \\
\partial_{i}^{2}\psi(\mathbf{x}_{k},t_{n}) \approx \left\{ [[\partial_{i}^{2}]]\psi^{n}\right\}_{k} := -\frac{1}{N_{i}} \sum_{p_{i}=-N_{i}/2}^{N_{i}/2-1} |\xi_{p_{i}}^{i}|^{2} \widetilde{\psi}_{\mathbf{k}|k_{i}\to p_{i}}^{n} e^{i\xi_{p_{i}}^{i}(x_{k_{i}}^{i}+L_{i})}. \tag{15}$$

In other words, for any $\alpha \in \mathbb{R}$ $c(\mathbf{x})\partial_i^{\alpha}u$ is approximated using its symbol $c(\mathbf{x})(\mathrm{i}\xi_i)^{\alpha}$ of the operator $c(\mathbf{x})\partial_i^{\alpha}$; that is by approximating $c(\mathbf{x})\mathcal{F}^{-1}\big((\mathrm{i}\xi_i)^{\alpha}\mathcal{F}(u)(\mathbf{x})\big)$.

Typically, when neglecting the high modes we get the following aliasing error estimates: for $\psi(\cdot,t) \in H^r$, there exists c>0 such that

$$\|\widetilde{\widetilde{\psi}} - \psi\|_{H^s} \leqslant c(N_1 N_2)^{s-r} \|\psi\|_{H^r},$$

for some r > s > 1 (in 2-d) and $\psi \in L^1 \cap H^r$ -periodic.

As discussed above, in the framework of photonic graphene, the material function (as well as the solution) is periodic in the direction v_1 (orthogonal to k_2) [18,22], for all $t \ge 0$

$$\psi(\mathbf{x} + \mathbf{v}_1, t) = \psi(\mathbf{x}, t)$$
.

while for $|\mathbf{x} \cdot \mathbf{k}_2| \to +\infty$ the solution tends to zero. In order to circumvent this issue in the direction \mathbf{v}_2 , we propose to use Perfectly Matched Layers (PML), allowing for absorbing the wavefunction in the direction \mathbf{v}_2 , while using a Fourier-based method. Typically, the idea consists in introducing an absorbing function S in the direction \mathbf{v}_2 . For the sake of simplicity, we could assume that \mathbf{v}_1 (resp. \mathbf{v}_2) is aligned with \mathbf{e}_x (resp. \mathbf{e}_y). Alternatively, a simple change of coordinates (corresponding to a rotation of angle $\pi/6$) can be applied as discussed below.

3.2. Survival kit on Perfectly Matched Layers (PML)

Let us recall the basics of PML [6,11,30]. The presentation is proposed on an one-dimensional bounded physical domain denoted by \mathcal{D}_{Phy} , as within the framework of this paper the PML will only be applied in one direction. We first add a layer which is called \mathcal{D}_{PML} , surrounding \mathcal{D}_{Phys} , stretching the *x*-coordinate. The overall computational domain is then defined by: $\mathcal{D} = \overline{\mathcal{D}_{Phy}} \cup \mathcal{D}_{PML}$. For the one-dimensional case, $\mathcal{D} = [-L, L]$ and $\mathcal{D}_{Phys} = [-L^*, L^*]$, with $L^* < L$ and stretching. PMLs require a complex stretching of the real spatial coordinate *x* such as

$$\widetilde{x}(x) = x + e^{i\theta} \int_{I^*}^{x} S(s)ds,$$
(16)

where the absorbing function $S: \mathcal{D} \to \mathbb{R}$ is defined as $(\alpha \in \mathbb{N}^*)$

$$S(x) = \begin{cases} s(|x| - L), & L^* \leq |x| < L, \\ 0, & |x| < L^*. \end{cases}$$
 (17)

The rotation angle θ is usually fixed by the problem under study. For example, $\theta = \pi/2$ is often considered for (integer order) time harmonic Helmholtz-type problems [12,29,30] while $\theta = \pi/4$ is more adapted to Schrödinger problems [4,6,31, 34]. Hence, we define first order damped operator as follows

$$\partial_x \mapsto \partial_{x_c} := (1 + e^{i\theta} S(x))^{-1} \partial_x$$

modifying hence the initial PDE. The same way for second order operator, we get

$$\partial_{x_c}^2 = (1 + e^{i\theta} S(x))^{-1} \partial_x ((1 + e^{i\theta} S(x))^{-1} \partial_x)$$

The choice of absorbing function is rather flexible. Typically for some $\delta_{x} > 0$,

Type I:
$$\sigma_0(x + \delta_x)^2$$
, Type II: $\sigma_0(x + \delta_x)^3$, Type III: $-\frac{\sigma_0}{x}$, Type IV: $\frac{\sigma_0}{x^2}$, Type V: $-\frac{\sigma_0}{x} - \frac{\sigma_0}{\delta_x}$, Type VI: $\frac{\sigma_0}{x^2} - \frac{\sigma_0}{\delta_x^2}$. (18)

We refer to [9] for details on PML.

3.3. The space-time discretization

In the following, we consider symmetry breaking functions of the form $\mathbf{W}(\mathbf{x}) = w(\mathbf{x})\mathbf{I}_{2\times 2}$. This typically corresponds to a \mathcal{P} -symmetry breaking, where, for instance, $w(\mathbf{x}) = a(\mathbf{x}) + \delta \eta(\mathbf{k}_2 \cdot \mathbf{x})b(\mathbf{x})$. The adaption to \mathcal{C} -symmetry breaking is straightforward. We set

$$S^{\delta} = -w(\mathbf{x}) \triangle - \nabla w(\mathbf{x}) \cdot \nabla + w(\mathbf{x}) \frac{k_{\parallel}^{2}}{4\pi^{2}} \|\mathbf{k}_{1}\|^{2} + i \left(-\frac{k_{\parallel}}{2\pi} \nabla w(\mathbf{x}) \cdot \mathbf{k}_{1} \right) - w(\mathbf{x}) \frac{k_{\parallel}}{2\pi} \mathbf{k}_{1} \cdot \nabla \right).$$

As we impose radiative condition in one direction (say e_y), and periodic boundary conditions in the orthogonal one (e_x), we propose to modify the equation under consideration introducing PML as discussed above.

We denote by $\Delta_S = \partial_x^2 + (1 + e^{\pm \theta})S(y))^{-1}\partial_y ((1 + e^{\pm \theta}S(y))^{-1}\partial_y)$ and $\nabla_S = (\partial_x, (1 + e^{\pm \theta}S(x))^{-1}\partial_y)^T$. Hence the operator S^{δ} is transformed as follows

$$S_S^{\delta} := -w(\mathbf{x}) \triangle_S - \nabla_S w(\mathbf{x}) \cdot \nabla_S + w(\mathbf{x}) \frac{k_{\parallel}^2}{4\pi^2} \|\mathbf{k}_1\|^2 + i \left(-\frac{k_{\parallel}}{2\pi} \nabla w(\mathbf{x}) \cdot \mathbf{k}_1 \right) - w(\mathbf{x}) \frac{k_{\parallel}}{2\pi} \mathbf{k}_1 \cdot \nabla_S \right).$$

Using the above notations and denoting by $\psi_h = \{\psi_i^n\}_{j,n}$ the approximate solution, we solve

$$i \partial_t \boldsymbol{\psi}_h = \left\{ -w(\boldsymbol{x}_h)[[\triangle_S]] - \nabla w(\boldsymbol{x}_h) \cdot [[\nabla_S]] + w(\boldsymbol{x}_h) \frac{k_\parallel^2}{4\pi^2} \|\boldsymbol{k}_1\|^2 \right. \\
\left. + i \left(-\frac{k_\parallel}{2\pi} \nabla w(\boldsymbol{x}_h) \cdot \boldsymbol{k}_1 \right) - w(\boldsymbol{x}_h) \frac{k_\parallel}{2\pi} \boldsymbol{k}_1 \cdot [[\nabla_S]] \right) \right\} \boldsymbol{\psi}_h.$$

The issue with the above approach is that it does not satisfy the periodicity in the correct direction imposed by the photonic graphene model (\mathbf{v}_1); but in the direction \mathbf{e}_x instead. In order to fix this problem, we can simply apply a change of variables as described below.

3.4. Change of coordinates

In order to include the periodic boundary conditions in the direction v_1 , it may be convenient to make the following change of variables obtained thanks to a rotation matrix \mathbf{R}' corresponding to the angle between \mathbf{e}_x and \mathbf{v}_1 . We denote by \mathbf{R}' the rotation matrix of angle $\pi/6$:

$$\mathbf{R}' = \frac{1}{2} \begin{pmatrix} \sqrt{3} & 1 \\ -1 & \sqrt{3} \end{pmatrix}.$$

Hence $\mathbf{e}_x = \mathbf{R}' \mathbf{v}_1$. We set $x' = (\sqrt{3}x + y)/2$ and $y' = (-x + \sqrt{3}y)/2$. Then

$$\partial_x = \frac{\sqrt{3}}{2} \partial_{x'} + \frac{1}{2} \partial_{y'}, \ \partial_y = -\frac{1}{2} \partial_{x'} + \frac{\sqrt{3}}{2} \partial_{y'},$$

and

$$\partial_{x}^{2} = \frac{3}{4}\partial_{x'}^{2} + \frac{1}{4}\partial_{y'}^{2} + \frac{\sqrt{3}}{2}\partial_{x'y'}, \ \ \partial_{y}^{2} = \frac{1}{4}\partial_{x'}^{2} + \frac{3}{4}\partial_{y'}^{2} - \frac{\sqrt{3}}{2}\partial_{x'y'}.$$

Moreover, $x = (\sqrt{3}x' - y')/2$ and $y = (x' + \sqrt{3}y')/2$. We then denote $\triangle' := \partial_{x'}^2 + \partial_{y'}^2$ and

$$\widetilde{w}(\mathbf{x}') := w((\sqrt{3}x' - y')/2, (x' + \sqrt{3}y')/2),$$

$$\nabla \widetilde{w}(\mathbf{x}') := \nabla w((\sqrt{3}x' - y')/2, (x' + \sqrt{3}y')/2).$$

Regarding the PML, we simply take S(y'). Similarly, we get from ∇_S

$$\nabla'_{\mathsf{S}} := \left(\frac{\sqrt{3}}{2}\partial_{\mathsf{X}'} + \frac{1}{2}\partial_{\mathsf{Y}'}, \left(1 + e^{\mathrm{i}\theta}\,\mathsf{S}(\mathsf{Y}')\right)^{-1} \left(-\frac{1}{2}\partial_{\mathsf{X}'} + \frac{\sqrt{3}}{2}\partial_{\mathsf{Y}'}\right)\right)^{\mathsf{T}}.$$

Finally, we define \triangle'_{S} as follows

$$\Delta'_{S} = \left(\frac{3}{4}\partial_{x'}^{2} + \frac{1}{4}\partial_{y'}^{2}\right) + \left(1 + e^{i\theta}S(y')\right)^{-1}\left(-\frac{1}{2}\partial_{x'} + \frac{\sqrt{3}}{2}\partial_{y'}\right)\left\{\left(1 + e^{i\theta}S(y')\right)^{-1}\left(-\frac{1}{2}\partial_{x'} + \frac{\sqrt{3}}{2}\partial_{y'}\right)\right\},\,$$

and

$$S_{S}^{\delta} = -\widetilde{w}(\mathbf{x}')\Delta_{S}' - \nabla\widetilde{w}(\mathbf{x}') \cdot \nabla_{S}' + \widetilde{w}(\mathbf{x}') \frac{k_{\parallel}^{2}}{4\pi^{2}} \|\mathbf{k}_{1}\|^{2} + i\left(-\frac{k_{\parallel}}{2\pi}\nabla\widetilde{w}(\mathbf{x}') \cdot \mathbf{k}_{1}\right) - \widetilde{w}(\mathbf{x}') \frac{k_{\parallel}}{2\pi} \mathbf{k}_{1} \cdot \nabla_{S}'\right).$$

Alternatively, we can consider a transformation mapping $(\mathbf{v}_1, \mathbf{v}_2)$ to $(\mathbf{e}_x, \mathbf{e}_y)$.

3.5. Time discretization and properties

The proposed approach will allow us to i) benefit from the accuracy and simplicity of Fourier-based methods, and ii) to absorb the wavefunction at the domain boundary when required. We denote by ψ_h^n the approximate solution at time t_n . We first introduce the following approximate pseudodifferential operator (we consider below the case of \mathcal{P} -symmetry breaking Schrödinger operator)

$$[[\mathcal{S}_{S}^{\delta}]] := -w(\mathbf{x})[[\triangle_{S}]] - \nabla w(\mathbf{x}_{h}) \cdot [[\nabla_{S}]] + w(\mathbf{x}_{h}) \frac{k_{\parallel}^{2}}{4\pi^{2}} \|\mathbf{k}_{1}\|^{2} + i\left(-\frac{k_{\parallel}}{2\pi} \nabla w(\mathbf{x}_{h}) \cdot \mathbf{k}_{1} - w(\mathbf{x}_{h}) \frac{k_{\parallel}}{2\pi} \mathbf{k}_{1} \cdot [[\nabla_{S}]]\right),$$

where the discrete operators $[[\Delta_S]]$ and $[[\nabla_S]]$ were introduced in the previous subsections. The time derivative can be treated using an backward Euler method, such as

$$\{I_N - i\Delta t[[\mathcal{S}_S^{\delta}]]\} \psi_h^{n+1} = \psi_h^n,$$

or a Crank-Nicolson based approximation

$$\left\{\frac{I_N}{2} + \mathrm{i}\,\frac{\Delta t}{2}[[\mathcal{S}_S^{\delta}]]\right\}\psi_h^{n+1} = \left\{\frac{I_N}{2} - \mathrm{i}\,\frac{\Delta t}{2}[[\mathcal{S}_S^{\delta}]]\right\}\psi_h^{n}.$$

It is easy to show the following result.

Proposition 3.1. For $\psi_0 \in L^2(\Lambda)$, we have the following stability results. The backward Euler scheme

$$\{I_N - i\Delta t[[\mathcal{S}_S^{\delta}]]\} \psi_h^{n+1} = \psi_h^n, \tag{19}$$

and the Crank-Nicolson scheme

$$\left\{ \frac{I_N}{2} + i \frac{\Delta t}{2} [[\mathcal{S}_S^{\delta}]] \right\} \psi_h^{n+1} = \left\{ \frac{I_N}{2} - i \frac{\Delta t}{2} [[\mathcal{S}_S^{\delta}]] \right\} \psi_h^n, \tag{20}$$

approximating (5) are unconditionally ℓ^2 -stable.

Proof. We denote $[[S^{\delta}]] = w(\mathbf{x}_h)[[\Delta]] + \nabla w(\mathbf{x}_h)[[\nabla]]$ for $k_{\parallel} = 0$. We consider the continuous case in $L^2(\mathbb{R}^2)$ and denote by \mathcal{F} and \mathcal{F}^{-1} the Fourier transform of a function $v \in L^2(\mathbb{R}^2)$. We denote $\boldsymbol{\xi} = (\xi_x, \xi_y)$ the Fourier variables associated to $\mathbf{x} = (x, y)$. Denoting by $\langle \cdot, \cdot \rangle$ the L^2 -inner product, we have

$$\begin{split} \langle \mathcal{S}^{\delta} \boldsymbol{v}, \boldsymbol{v} \rangle &= \langle \boldsymbol{w}(\boldsymbol{x}) \mathcal{F}^{-1}(-|\boldsymbol{\xi}|^2 \mathcal{F}(\boldsymbol{v})), \mathcal{F}^{-1}(\mathcal{F}(\boldsymbol{v})) \rangle + \langle \boldsymbol{w}_{\boldsymbol{x}}(\boldsymbol{x}) \mathcal{F}^{-1}(\mathrm{i}\boldsymbol{\xi}_{\boldsymbol{x}} \mathcal{F}(\boldsymbol{v})), \mathcal{F}^{-1}(\mathcal{F}(\boldsymbol{v})) \rangle \\ &+ \langle \boldsymbol{w}_{\boldsymbol{y}}(\boldsymbol{x}) \mathcal{F}^{-1}(\mathrm{i}\boldsymbol{\xi}_{\boldsymbol{y}} \mathcal{F}(\boldsymbol{v})), \mathcal{F}^{-1}(\mathcal{F}(\boldsymbol{v})) \rangle \\ &= \langle \boldsymbol{w}(\boldsymbol{x}) \partial_{\boldsymbol{x}}^2 \boldsymbol{v}, \boldsymbol{v} \rangle + \langle \boldsymbol{w}(\boldsymbol{x}) \partial_{\boldsymbol{y}}^2 \boldsymbol{v}, \boldsymbol{v} \rangle + \langle \boldsymbol{w}_{\boldsymbol{x}}(\boldsymbol{x}) \partial_{\boldsymbol{x}} \boldsymbol{v}, \partial_{\boldsymbol{x}} \boldsymbol{v} \rangle + \langle \boldsymbol{w}_{\boldsymbol{y}}(\boldsymbol{x}) \partial_{\boldsymbol{y}} \boldsymbol{v}, \partial_{\boldsymbol{y}} \boldsymbol{v} \rangle \\ &= -\langle \partial_{\boldsymbol{x}}(\boldsymbol{w}(\boldsymbol{x}) \partial_{\boldsymbol{x}}) \boldsymbol{v}, \boldsymbol{v} \rangle - \langle \partial_{\boldsymbol{y}}(\boldsymbol{w}(\boldsymbol{x}) \partial_{\boldsymbol{y}}) \boldsymbol{v}, \partial_{\boldsymbol{y}} \boldsymbol{v} \rangle \\ &= -\langle \boldsymbol{w}(\boldsymbol{x}) \mathcal{F}^{-1}(\mathrm{i}\boldsymbol{\xi}_{\boldsymbol{x}} \mathcal{F}(\boldsymbol{v})), \mathcal{F}^{-1}(\mathrm{i}\boldsymbol{\xi}_{\boldsymbol{x}} \mathcal{F}(\boldsymbol{v})) \rangle - \langle \boldsymbol{w}(\boldsymbol{x}) \mathcal{F}^{-1}(\mathrm{i}\boldsymbol{\xi}_{\boldsymbol{y}} \mathcal{F}(\boldsymbol{v})), \mathcal{F}^{-1}(\mathrm{i}\boldsymbol{\xi}_{\boldsymbol{y}} \mathcal{F}(\boldsymbol{v})) \rangle \,. \end{split}$$

Similarly at the discrete level, denoting $\mathbf{v}_h \in \ell^2$ and $\langle \cdot , \cdot \rangle_h$ the ℓ^2 -inner product, we get

$$\begin{split} \langle [[\mathcal{S}^{\delta}]] \boldsymbol{v}_h, \boldsymbol{v}_h \rangle_h &= \langle w(\boldsymbol{x}_h) \mathcal{F}_h^{-1}(-|\boldsymbol{\xi}_h|^2 \mathcal{F}_h(\boldsymbol{v}_h)), \mathcal{F}_h^{-1}(\mathcal{F}_h(\boldsymbol{v}_h)) \rangle_h \\ &+ \langle w_{\boldsymbol{x}}(\boldsymbol{x}_h) \mathcal{F}_h^{-1}(\mathrm{i}\boldsymbol{\xi}_{\boldsymbol{x};h} \mathcal{F}_h(\boldsymbol{v}_h)), \mathcal{F}_h^{-1}(\mathcal{F}_h(\boldsymbol{v}_h)) \rangle_h \\ &+ \langle w_{\boldsymbol{y}}(\boldsymbol{x}_h) \mathcal{F}_h^{-1}(\mathrm{i}\boldsymbol{\xi}_{\boldsymbol{y};h} \mathcal{F}_h(\boldsymbol{v}_h)), \mathcal{F}_h^{-1}(\mathcal{F}_h(\boldsymbol{v}_h)) \rangle_h \\ &= - \langle w(\boldsymbol{x}_h) \mathcal{F}_h^{-1}(\mathrm{i}\boldsymbol{\xi}_{\boldsymbol{x};h} \mathcal{F}_h(\boldsymbol{v}_h)), \mathcal{F}_h^{-1}(\mathrm{i}\boldsymbol{\xi}_{\boldsymbol{x};h} \mathcal{F}_h(\boldsymbol{v}_h)) \rangle_h \\ &- \langle w(\boldsymbol{x}_h) \mathcal{F}_h^{-1}(\mathrm{i}\boldsymbol{\xi}_{\boldsymbol{y};h} \mathcal{F}_h(\boldsymbol{v}_h)), \mathcal{F}_h^{-1}(\mathrm{i}\boldsymbol{\xi}_{\boldsymbol{y};h} \mathcal{F}_h(\boldsymbol{v}_h)) \rangle_h \,. \end{split}$$

Considering the Crank-Nicolson-based algorithm, and assuming $\|\psi_h^n\|_2 \leqslant C \|\psi_h^0\|_2$, we multiply by $\overline{\psi}_h^{n+1}$ and integrate to get

$$\left\langle \left\{ \frac{I_N}{2} - \mathrm{i} \frac{\Delta t}{2} [[\mathcal{S}_S^{\delta}]] \right\} \psi_h^{n+1}, \psi_h^{n+1} \right\rangle_h = \left\langle \left\{ \frac{I_N}{2} + \mathrm{i} \frac{\Delta t}{2} [[\mathcal{S}_S^{\delta}]] \right\} \psi_h^{n}, \psi_h^{n+1} \right\rangle_h.$$

Then

$$|\boldsymbol{\psi}_h^{n+1}|_h^2 - \mathrm{i} \Delta t \big\langle [[\mathcal{S}_S^{\delta}]] \boldsymbol{\psi}_h^{n+1}, \boldsymbol{\psi}_h^{n+1} \big\rangle_h = \langle \boldsymbol{\psi}_h^n, \boldsymbol{\psi}_h^{n+1} \rangle_h + \mathrm{i} \Delta t \big\langle [[\mathcal{S}_S^{\delta}]] \boldsymbol{\psi}_h^n, \boldsymbol{\psi}_h^{n+1} \rangle_h.$$

From the above computation and taking the real part of the equation, we get

$$\begin{aligned} |\boldsymbol{\psi}_{h}^{n+1}|_{h}^{2} + \Delta t \operatorname{Im} \langle [[\mathcal{S}_{S}^{\delta}]] \boldsymbol{\psi}_{h}^{n+1}, \boldsymbol{\psi}_{h}^{n} \rangle_{h} &= \operatorname{Re} \langle \boldsymbol{\psi}_{h}^{n}, \boldsymbol{\psi}_{h}^{n+1} \rangle_{h} \\ &\leq \frac{1}{2} |\boldsymbol{\psi}_{h}^{n+1}|_{h}^{2} + \frac{1}{2} |\boldsymbol{\psi}_{h}^{n}|_{h}^{2}. \end{aligned}$$

Then, we easily deduce that

$$| {\pmb \psi}_h^{n+1} |_h^2 \, \leqslant \, | {\pmb \psi}_h^{n} |_h^2 + O(\Delta t^2) \, .$$

Hence, at any time T_n

$$|\psi_h^n|_h^2 \leqslant |\psi_h^0|_h^2 + O(T_n\Delta t),$$

which concludes the proof. \Box

3.6. Feit-Fleck method for edge state computation

It is simple to adapt the time-dependent solver developed above for constructing eigenfunctions (edge-states) to the operator $-\nabla \cdot (\boldsymbol{W}(\boldsymbol{x})\nabla)$. A standard Feit-Fleck-like algorithm [16] is proposed hereafter. The computation of edge state energies are non-trivial as they are usually located in a spectral gap which is usually analytically unknown. Hence a direct minimization of the Rayleigh coefficient, the use of Galerkin method, or even finite difference approximation usually leads to spectral pollution or/and dissolution in the continuum [14,15]. Feit-Fleck methods allow to avoid this type of issues. Let us introduce an arbitrary trial function

$$\psi_0(\mathbf{x}) = \sum_n c_n \phi_n(\mathbf{x}) \,, \tag{21}$$

where $\{c_n\}_n$ is a sequence of unknown complex numbers, and $\{\phi_n\}_n$ is the sequence of unknown orthogonal "eigenfunctions" (including edge states). If we denote ψ_ℓ the exact solution to the corresponding time-dependent Schrödinger equation, we get

$$\psi_e(\mathbf{x},t) = \sum_n c_n \exp(-iE_n t)\phi_n(\mathbf{x}). \tag{22}$$

We next denote the exact autocorrelation function by

$$C_e(t) = \langle \psi_e(\cdot, t), \psi_0 \rangle = \sum_n |c_n|^2 \exp(-iE_n t).$$

We now denote by $\hat{\cdot}$ the Fourier transform in time. Hence the exact Fourier transform provides the power spectrum of the operator:

$$\widehat{C}_e(E) = \sum_n |c_n|^2 \delta_0(E - E_n).$$

When apply to say $\chi \in \mathcal{C}^{\infty}(\mathbb{R})$, we then get

$$\langle \widehat{C}_e, \chi \rangle_E = \sum_n |c_n|^2 \chi(E_n).$$

Hence, the edge state energies will correspond to the peaks in the graph of the $|\widehat{C}_e|^2$. Denoting ψ_h the approximate solution and C_h the corresponding approximate auto-correlation function. For any $\chi \in \mathcal{C}_0^{\infty}(\mathbb{R})$ (C^{∞} with compact support functions), we get

$$\begin{array}{l} \left| \langle \widehat{C}_e, \chi \rangle_E - \langle \widehat{C}_h, \chi \rangle_E \right| \leq \left| \int_{\mathbb{R}} \chi(E) \int e^{\mathrm{i} t \tau} (C_e(t) - C_h(t)) dt dE \right| \\ \leq \left| \int_{\mathbb{R}} \chi(E) \int e^{\mathrm{i} t E} \langle \psi_0, \psi_e(\cdot, t) - \psi_h(\cdot, t) \rangle dt dE \right| \\ \leq \sup_E \|\widehat{\psi}_e(\cdot, E) - \widehat{\psi}_h(\cdot, E)\|_{L_x^2} \|\psi_0\|_{L_x^2} \|\chi\|_{L^1(\mathbb{R})} \,. \end{array}$$

This estimate is not very sharp and in order to determine $\widehat{C}(E)$, the wavefunction should be evolved to infinite time which is practically difficult. Hence, instead of computing C_e for all t, we will solve the time-dependent Schrödinger equation on a finite interval [0,T] and compute the FFT of $C^{(w_T)}(t) := C(t)w_T(t)$ for some window function w_T , in order to obtain the power spectrum by fitting the peaks with the lineshape. Practically, Hanning's functions are often chosen (see also [13,17] in the case of the Dirac operator)

$$w_T(t) = \begin{cases} \frac{1 - \cos\left(\frac{2\pi t}{T}\right)}{T}, & \text{for } t \in [0, T], \\ 0, & \text{for } t \in (-\infty, 0) \cup (T, \infty). \end{cases}$$

$$(23)$$

Once the egde state energy $E_{\rm es}$, is calculated, the corresponding approximate eigenstate $\psi_{\rm es}$ can be obtained by using

$$\psi_{\text{es}}(\mathbf{x}) = \int_{0}^{T} dt \psi(\mathbf{x}, t) w(t) e^{iE_{\text{es}}t}, \tag{24}$$

where $\psi(\mathbf{x}, 0)$ is an arbitrary trial function. This can be justified thanks to the lineshape function \mathcal{T} [16],

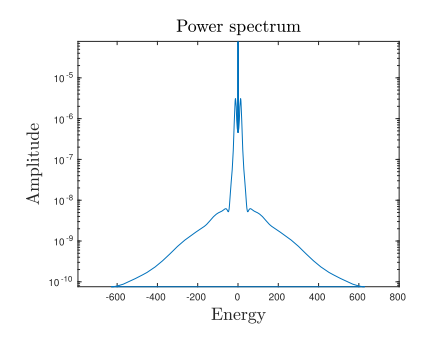
$$\mathcal{T}(E - E_n) = \int_{0}^{T} \exp\left(i(E - E_n)t\right) w(t) dt.$$

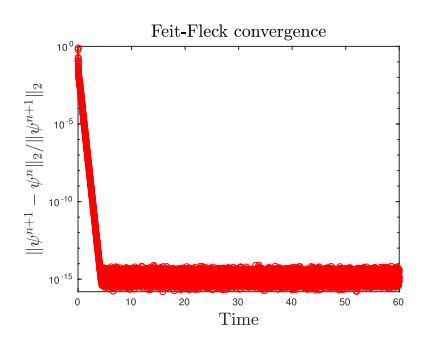
Notice that this method is not directly applicable to compute degenerate states. Let us conclude by mentioning that the energy resolution is given by $\Delta E_{\min} = \pi/T$ and the maximum bandwidth $\Delta E_{\max} = \pi/\Delta t$ ([16]).

Experiment 0. Let us consider a simple example to illustrate the construction of edge states with a Feit-Fleck method, for $\alpha \mathcal{L}$, where $\alpha = 0.075$. The computational domain is $[-\pi, \pi] \times [-2\pi, 2\pi]$ and the initial data is

$$\psi_0(\mathbf{x}) = \exp\left(-5\|\mathbf{x}\|^2\right)/N_0,$$

where N_0 is a normalization constant ($\|\psi_0\|_2 = 1$). We choose the following medium function





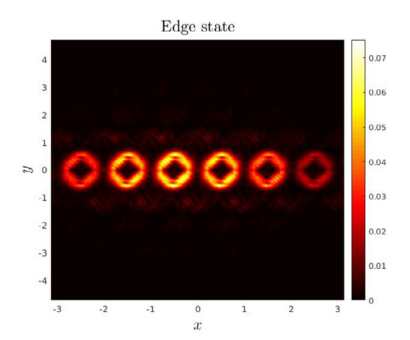


Fig. 5. (Left) Power spectrum. (Middle) Feit-Fleck convergence $\|\psi^{n+1} - \psi^n\|_2 / \|\psi^{n+1}\|_2$ as function of time. (Right) Edge state modulus.

$$a(\mathbf{x}) = 5 - \sum_{i=1}^{3} \cos(\mathbf{k}_i \cdot \mathbf{x}), \qquad (25)$$

and the wall function is defined by

$$w(\mathbf{x}) = \delta_1 \tanh(\delta_2 \mathbf{k}_2 \cdot \mathbf{x}) \sum_{i=1}^3 \sin(\mathbf{k}_i \cdot \mathbf{x}),$$

with $\delta_1 = 1.5$ and $\delta_2 = 30$. We compute the solution and the correlation function C over [0, T] with T = 100, and a time step given by $\Delta t = 5 \times 10^{-3}$ and $N_x = N_y = 121$. We report in Fig. 5 the spectrum of C and the edge state corresponding to the energy peak at 40.7. Then we solve a second time the equation in order to approximate the corresponding eigenfunction as proposed in (24), and denoted ψ_{es} . Once the rotation is performed (see Subsection 3.4), the wall function is located at $\gamma = 0$.

In order to illustrate the propagation of edge states along the wall, we perturb the computed edge state, by a Gaussian function centered at $\mathbf{x}_0 = (2.5, 0)$,

$$\phi_0(\mathbf{x}) = \psi_{es}(\mathbf{x}) \exp(-10\|\mathbf{x} - \mathbf{x}_0\|^2)/N_0$$
,

where N_0 is a normalization constant. We report the solutions at time t = 0, 1.25, 2.5, 3.75, 5 illustrating, as expected the propagation along the wall (see Fig. 6).

4. Numerical experiments

This section is dedicated to numerical experiments. In the first experiment, we simply check some basic properties of the computational method. Then we propose some more advanced physical simulations. In particular, we exhibit an edge-state like behavior along a wall in the photonic graphene and a trapping phenomenon as described in Section 2.

Experiment 1. In the first experiment, we propose a simple illustration of the PML-based pseudospectral method by testing the absorption of a wavefunction in the absorbing layer. The computational domain is $[-\pi, \pi]^2$ and the initial data is

$$\psi_0(\mathbf{x}) = \exp\left(-\gamma \|\mathbf{x} - \mathbf{x}_0\|^2 + \mathrm{i}\mathbf{k}_0 \cdot \mathbf{x}\right) / N_0,$$

where N_0 is a normalization constant ($\|\psi_0\|_2 = 1$). As a preliminary calculation, we check that the ℓ^2 -norm of the solution is properly conserved when there is no interaction with the boundary, using a Crank-Nicolson based algorithm. In this goal, we first take the center of the Gaussian at $\mathbf{x}_0 = (0,0)$ and $\mathbf{k}_0 = (2,2)^T$ (and $\alpha = 0.1$, $\zeta = 0$ in (26)), we compute the solution for $t \in [0,4]$, and we report $1 - \|\psi_h^n\|_2$ in logscale, as a function of t_n in Fig. 7 (Top-Left). We observe that the ℓ^2 -norm is accurately conserved.

Then, we compare the solution with and without PML for $\mathbf{k}_0 = (0, 20)^T$, $\mathbf{x}_0 = (0, 2.25)$ and $\gamma = 30$. We use the PML of type VI (18), see Section 3, and we consider the following material function

$$a(\mathbf{x}) = \alpha + \beta \sum_{i=1}^{3} \cos(\zeta \, \mathbf{k}_i \cdot \mathbf{x}), \tag{26}$$

where $\alpha=0.02$, $\beta=0.004$, $\zeta=0.1$. The wavefunction function is driven out from the domain through the upper boundary $\{y=\pi\}$. The PML size is taken equal to 7.5% in the y-direction, and is located in the zone $\Omega\setminus\Omega_{PML}=[-\pi,\pi]\times[0.925\pi,\pi]$. We report the ℓ^2 -norm of the overall approximate PML and no-PML solutions ψ_h^n at any time t_n , that is $\|\psi_h^n\|_2$ in the zone excluding the PML, $\Omega\setminus\Omega_{PML}$ (to get a rigorous comparison). In other words in both cases, we expect the solution ℓ^2 -norm

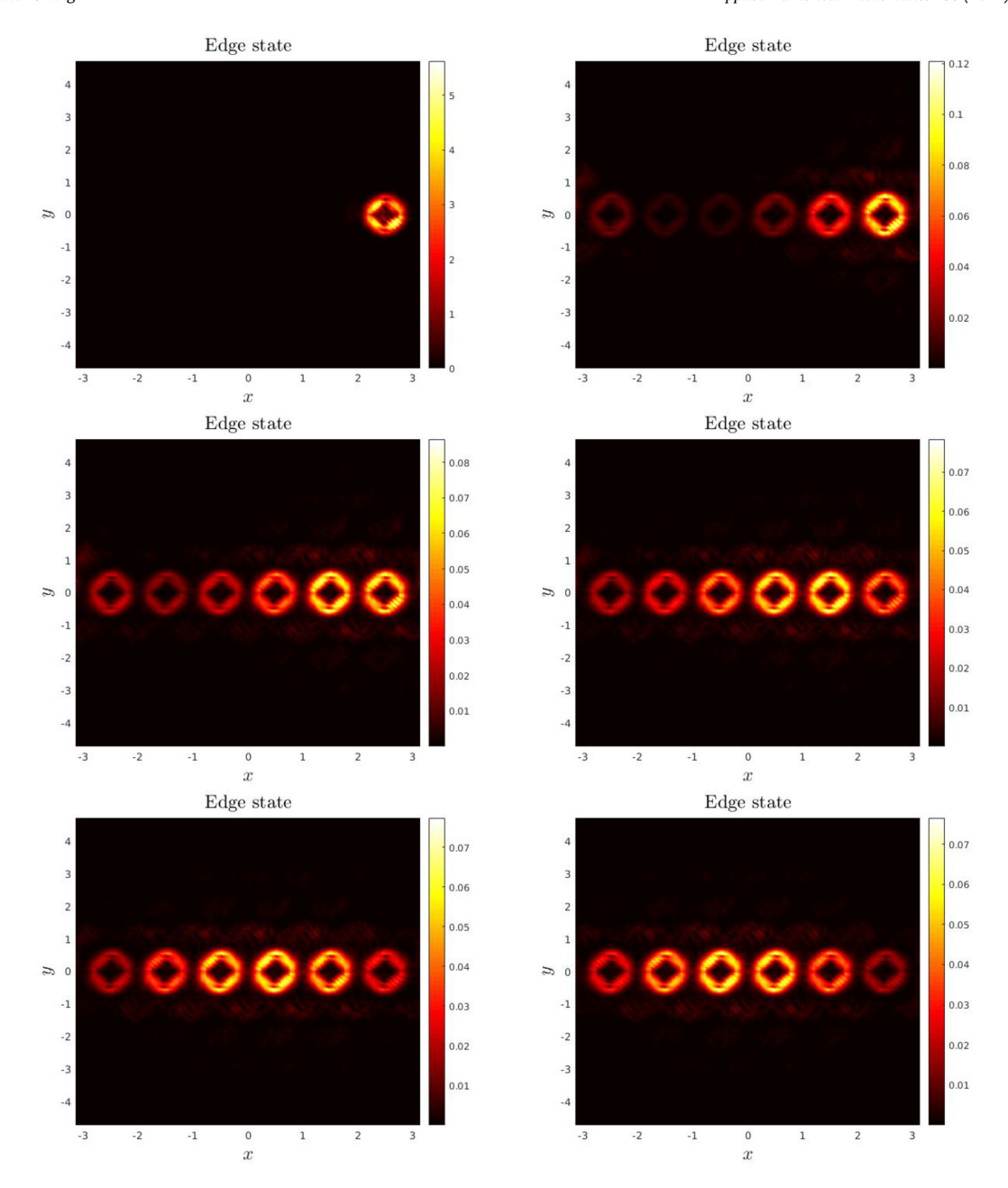


Fig. 6. From Top-Left to Bottom-Right: wavefunction propagation from for t = 0, 125, 2.5, 3.75, 5, 6.125.

to decrease (as entering the layer); but only in presence of PML is the solution really absorbed. Without PML the solution is eventually periodically transmitted through the top boundary, and its ℓ^2 -norm will increase and eventually get close to 1. It is expected in the first case, that the ℓ^2 -norm will go to zero (absorption) unlike the solution without PML. The latter will allow to mainly avoid the propagation of unphysical waves through periodic boundary conditions. The computation data are the following $N_x = N_y = 101$, and $\delta = 0.025$.

We report in Fig. 7 the solution at time T=2 without PML (standard periodic boundary conditions, Top-Right) and with PML (Bottom-Left). We plot in Fig. 7 (Bottom-Right) the overall ℓ^2 -norm as a function of time, illustrating the absorption when using PML.

Experiment 2. In this experiment, we are interested in the capture by a *curved* wall of a wavefunction in the case of C-symmetry breaking. We compare the evolution of the wavefunction with or without wall. We propose the following material function w

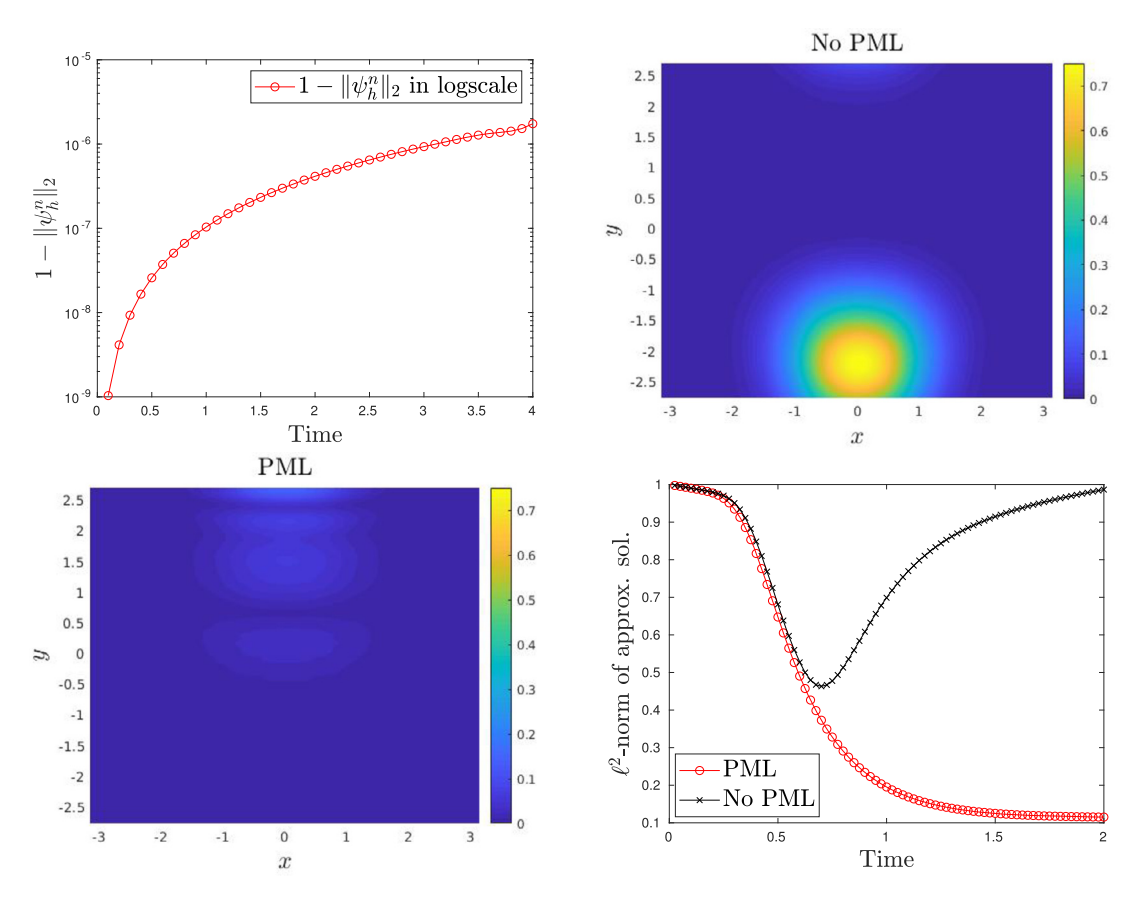


Fig. 7. Experiment 1. (Top-Left) ℓ^2 -norm conservation as function of time without boundary interaction. (Top-Right) Wavefunction without PML. (Bottom-Left) Wavefunction with PML in the *y*-direction. (Bottom-Right) ℓ^2 -norm as function of time.

$$w(\mathbf{x}) = a + b \sum_{i=1}^{3} \sin(\mathbf{k}_{i} \cdot \mathbf{x}) + \delta_{1} \eta(\delta_{2} \mathbf{k}_{2} \cdot \mathbf{x}) \sum_{i=1}^{3} \cos(\delta_{3} \mathbf{k}_{i} \cdot \mathbf{x}) + k_{\parallel} \left(w(\mathbf{x}) \frac{k_{\parallel}}{4\pi^{2}} ||\mathbf{k}_{1}||^{2} + i \left(-\frac{1}{2\pi} \nabla w(\mathbf{x}) \cdot \mathbf{k}_{1} \right) - w(\mathbf{x}) \frac{1}{2\pi} \mathbf{k}_{1} \cdot \nabla \right) \right),$$

$$(27)$$

with $\eta = \tanh$ and where a = 0.05, b = 0.01, $\delta_1 = 3$, $\delta_2 = 2$ and $\delta_3 = 0.22$, $k_{\parallel} = 0$. The choice of these parameters allows for a larger flexibility to construct relevant benchmarks. In order to exhibit the effect of the perturbation, we will also consider a low dispersion case. The initial data is given by

$$\psi_0(\mathbf{x}) = \exp\left(-\gamma \|\mathbf{x} - \mathbf{x}_0\|^2\right) / N_0,$$

with $\gamma=20$ (resp. 10) and $\mathbf{x}_0=(\pi/2,20\pi/17)$. The solution is computed from time 0 to T=0.02. We consider the following numerical data $\Delta t=0.0001$, $N_x=N_y=151$. On Fig. 8, we report the normalized restriction of the solution $\psi_{\text{Wall}}=\psi_{\mid \mathcal{N}_W}$ with $\varepsilon=0.9$ (9), as well as in Fig. 9 the solution at times T=0.01 (Left) and T=0.02 (Middle). We also report the propagation of the maximum of the solution as a function of time, see Fig. 9 (Right).

We observe that the wavefunction is mainly trapped in a disc, as it was expected from the discussion proposed in Section 2. At further times, the wavefunction which propagates along the wall is also eventually stopped, see Fig. 10 where is reported the solution at T = 0.035. This phenomenon can be interpreted by looking at Fig. 11 (Left): at the intersection of the wall and the level set (circle) $w(\mathbf{x}) = 0$. More specifically, the boundary of these discs is defined as the following sets

$$C := \left\{ \boldsymbol{x} \in \Lambda / \sum_{i=1} \cos(\delta_3 \boldsymbol{k}_i \cdot \boldsymbol{x}) = 0 \right\}.$$
 (28)

That is the wavefunction stops propagating for $x \in C \cap W$, where

$$W := \left\{ \boldsymbol{x} \in \Lambda / \boldsymbol{k}_2 \cdot \boldsymbol{F}(\boldsymbol{x}) = 0 \right\}.$$

This also corresponds to a region where w_x and w_y are close to 0, see (11) (Right) and the velocity vector field is almost null along the wall. To allow the wavefunction to continue its propagation along the wall, it is necessary to avoid the diffusion

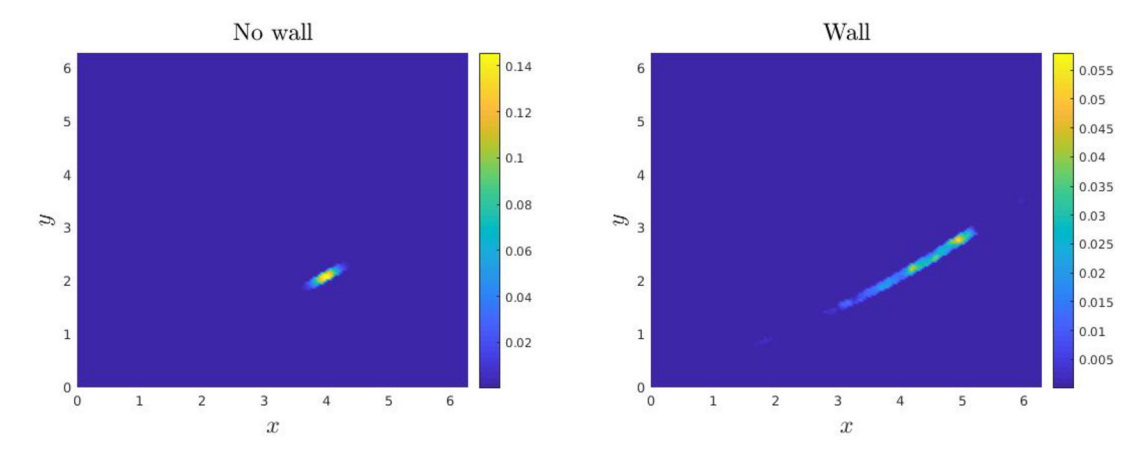


Fig. 8. Experiment 2. Normalized restriction on the wall of the wavefunction at time T = 0.01 (Left) without wall. (Right) with wall.

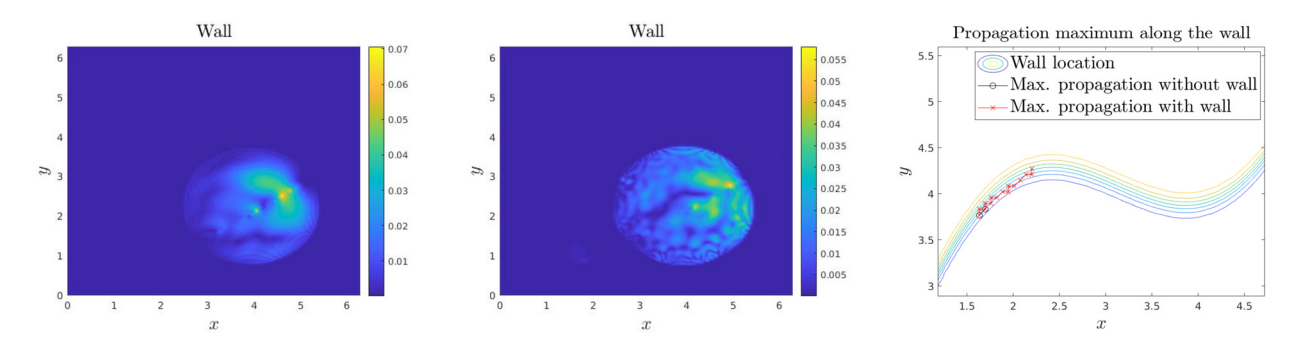


Fig. 9. Experiment 2. (Left) Wavefunction at time T = 0.01. (Middle) At time T = 0.02 (Right) Position of wavefunction maximum as function of time.

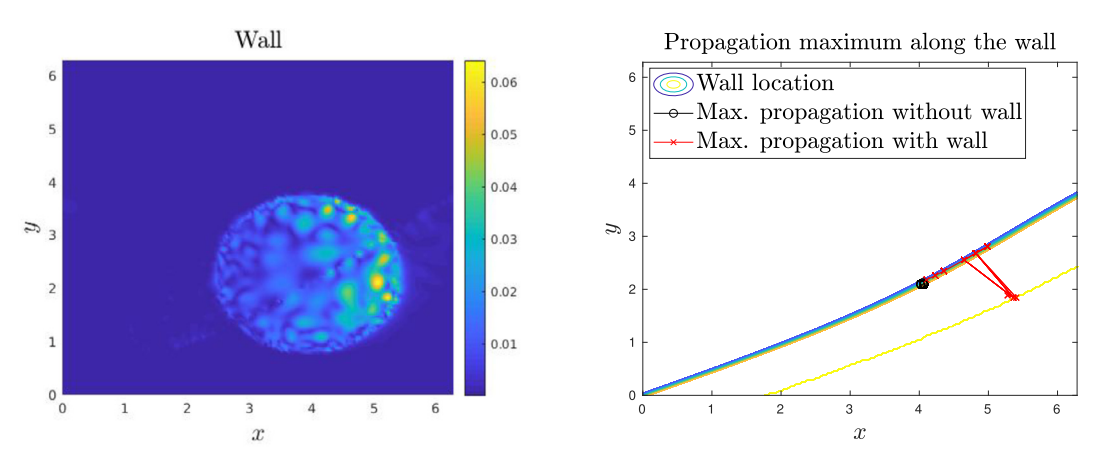


Fig. 10. Experiment 2. (Left) Wavefunction at time T = 0.035. (Right) Position of wavefunction maximum as function of time.

zone, or alternatively to take δ_3 smaller in (27). By continuity arguments, the behavior presented in this experiment is expected to remain valid for $k_{\parallel} \neq 0$, at least small.

Experiment 3. In this experiment, we are interested in the propagation of the wavefunction towards the wall again in the case of C-symmetry breaking. We start with an initial data located far from the wall, with a non-zero momentum

$$\psi_0(\mathbf{x}) = \exp\left(-\gamma \|\mathbf{x} - \mathbf{x}_0\|^2 + \mathrm{i}\mathbf{k}_0 \cdot \mathbf{x}\right)/N_0,$$

with $\mathbf{k}_0 = (0, -5)^T$, $\mathbf{x}_0 = (4, 3)$, $\gamma = 40$. The initial state is then located inside C defined in (28). In (27) we take $\eta = \tanh$ and a = 0.1, b = 0.1, $\delta_1 = 6$, $\delta_2 = 2$ and $\delta_3 = 0.22$. We observe that the wavefunction, as expected, remains inside C as

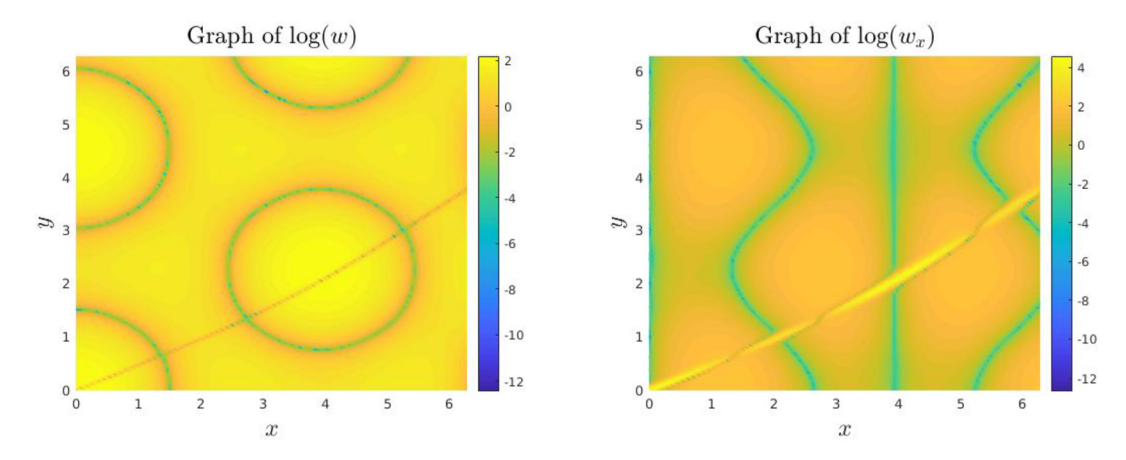


Fig. 11. Experiment 2. Graph of $\log |w|$, $\log |w_x|$.

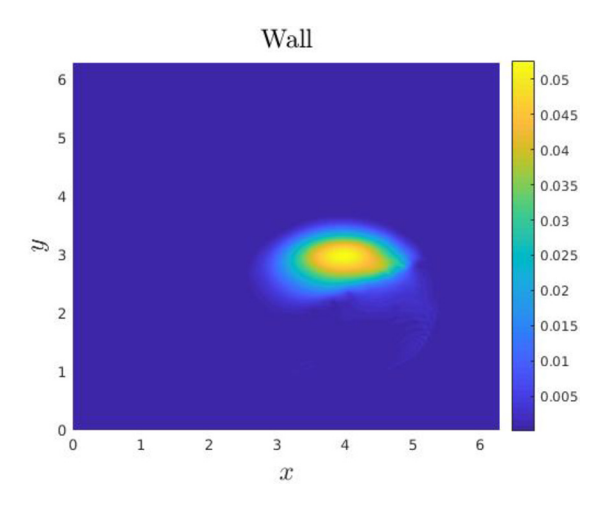


Fig. 12. Experiment 3. Wavefunction at final time.

reported in Fig. 12. We refer this phenomenon as a trapping of the wavefunction, and which could have some potential applications in photonics and optics.

Experiment 4. In this experiment, we are interested in the propagation of wavefunctions in the case of \mathcal{P} -symmetry breaking. Unlike the \mathcal{C} -symmetry breaking case, the propagation along the wall is negligible, see Section 2. We compare the evolution of a wavefunction with or without wall. In particular, in order to exhibit the effect of the perturbation, we will again consider a low dispersion case,

$$w(\mathbf{x}) = a + b \sum_{i=1}^{3} \sin(\mathbf{k}_{i} \cdot \mathbf{x}) + \delta_{1} \eta(\delta_{2} \mathbf{k}_{2} \cdot \mathbf{x}) \sum_{i=1}^{3} \cos(\delta_{3} \mathbf{k}_{i} \cdot \mathbf{x}),$$

 $\eta(\mathbf{x}) = \tanh(\mathbf{k}_2 \cdot \mathbf{F}(\mathbf{x}))$ where a = 0.025, b = 0.01, $\delta_1 = 3$, $\delta_2 = 2$ and $\delta_3 = 0.25$. The initial data is given by

$$\psi_0(\mathbf{x}) = \exp\left(-\gamma \|\mathbf{x} - \mathbf{x}_0\|^2\right) / N_0,$$

with $\gamma=20$ and $\mathbf{x}_0=(3,\sqrt{3})$ (resp. $(\pi/2,20\pi/17)$). The solution is computed from time 0 to T=0.3. We consider the following numerical data $\Delta t=0.0001$, $N_x=N_y=151$. On Fig. 13 (Left), we report the propagation of the maximum of the solution as a function of time Fig. 13 (Right). We observe a weak propagation along the wall, which is consistent with the analysis presented in the \mathcal{P} -symmetry case in Section 2.

5. Concluding remarks

In this paper, we have proposed one of the first numerical studies of the dynamics of wavefunctions in photonic graphene for complex materials. We have developed a pseudospectral method combined with directional perfect matched layers in this goal. The proposed method allows us to compute edge states (thanks to a Feit-Fleck-like method) and their dynamics,

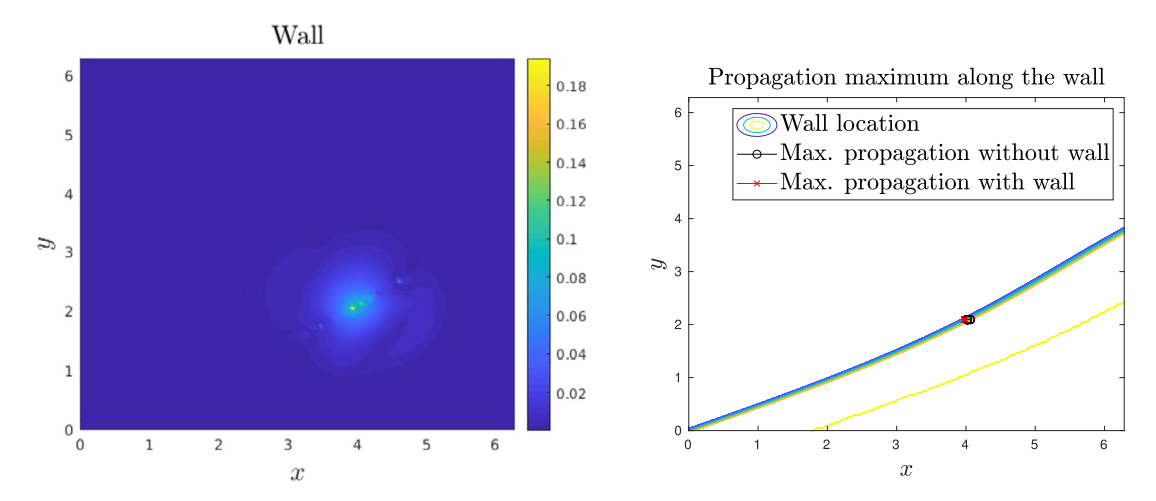


Fig. 13. Experiment 4. (Left) Wavefunction at time T = 0.3. (Right) Position of wavefunction maximum as function of time.

and more generally, the dynamics of any wavefunction within photonic graphene. In particular, we have mathematically and numerically exhibited an interesting trapping phenomenon, and derived equivalent equations in the vicinity and away from walls. In future work, we plan to explore in more detail the physical properties of edge states in photonic graphene.

Acknowledgement

E.L. was partially supported by NSERC through the Discovery Grant program. X.Y. was partially supported by the NSF grants DMS-1818592 and DMS-2109116. This research was conducted while E.L. was visiting the Department of Mathematics of the University of California Santa Barbara, and the Institute of Pure and Applied Mathematics at the University of California Los Angeles. E.L. would like in particular to thank both institutions for the financial and administrative supports.

References

- [1] X. Antoine, E. Lorin, Computational performance of simple and efficient sequential and parallel Dirac equation solvers, Comput. Phys. Commun. 220 (2017) 150–172.
- [2] X. Antoine, E. Lorin, A simple pseudospectral method for the computation of the time-dependent Dirac equation with perfectly matched layers, J. Comput. Phys. 395 (2019) 583–601.
- [3] X. Antoine, E. Lorin, Towards perfectly matched layers for time-dependent space fractional PDEs, J. Comput. Phys. 391 (2019) 59–90.
- [4] X. Antoine, A. Arnold, C. Besse, M. Ehrhardt, A. Schaedle, A review of transparent and artificial boundary conditions techniques for linear and nonlinear Schroedinger equation, Commun. Comput. Phys. 4 (4) (2008) 729–796.
- [5] X. Antoine, C. Besse, V. Rispoli, High-order IMEX-spectral schemes for computing the dynamics of systems of nonlinear Schrödinger/Gross-Pitaevskii equations, J. Comput. Phys. 327 (2016) 252–269.
- [6] X. Antoine, E. Lorin, Q. Tang, A friendly review of absorbing boundary conditions and perfectly matched layers for classical and relativistic quantum waves equations, Mol. Phys. 115 (15–16) (2017) 1861–1879.
- [7] X. Antoine, C. Geuzaine, Q. Tang, Perfectly matched layer for computing the dynamics of nonlinear Schrödinger equations by pseudospectral methods. Application to rotating Bose-Einstein condensates, Commun. Nonlinear Sci. Numer. Simul. 90 (2020) 105406, https://doi.org/10.1016/j.cnsns.2020.
- [8] X. Antoine, E. Lorin, Y. Zhang, Derivation and analysis of computational methods for fractional Laplacian equations with absorbing layers, Numer. Algorithms 87 (1) (2021) 409–444.
- [9] E. Bécache, A.-S. Bonnet-Ben Dhia, G. Legendre, Perfectly matched layers for the convected Helmholtz equation, SIAM J. Numer. Anal. 42 (1) (2004) 409–433.
- [10] J.J. Benito, F. Ureña, L. Gavete, E. Salete, A. Muelas, A GFDM with PML for seismic wave equations in heterogeneous media, J. Comput. Appl. Math. 252 (2013) 40–51.
- [11] J.-P. Bérenger, A perfectly matched layer for the absorption of electromagnetic waves, J. Comput. Phys. 114 (2) (1994) 185–200.
- [12] A. Bermúdez, L. Hervella-Nieto, A. Prieto, R. Rodríguez, An exact bounded perfectly matched layer for time-harmonic scattering problems, SIAM J. Sci. Comput. 30 (2007) 312–338.
- [13] Y. Cai, E. Lorin, Stationary state computation for nonlinear Dirac operators, J. Comput. Phys. 420 (2020) 109679.
- [14] J. Dolbeault, M.J. Esteban, E. Séré, On the eigenvalues of operators with gaps. Application to Dirac operators, J. Funct. Anal. 174 (1) (2000) 208–226.
- [15] J. Dolbeault, M.J. Esteban, E. Séré, Variational characterization for eigenvalues of Dirac operators, Calc. Var. Partial Differ. Equ. 10 (2000) 321–347.
- [16] M.D. Feit, J.A. Fleck Jr., A. Steiger, Solution of the Schrödinger equation by a spectral method, J. Comput. Phys. 47 (3) (1982) 412-433.
- [17] F. Fillion-Gourdeau, E. Lorin, A.D. Bandrauk, Numerical solution of the time-dependent Dirac equation in coordinate space without fermion-doubling, Comput. Phys. Commun. 183 (7) (2012) 1403–1415.
- [18] H. Guo, X. Yang, J. Comput. Phys. (2021).
- [19] P. Hu, L. Hong, Y. Zhu, Linear and nonlinear electromagnetic waves in modulated honeycomb media, Stud. Appl. Math. (2019).
- [20] P.S. Jung, G.G. Pyrialakos, F.O. Wu, M. Parto, M. Khajavikhan, W. Krolikowski, D.N. Christodoulides, Thermal control of the topological edge flow in nonlinear photonic lattices, Nat. Commun. 13 (1) (2022).
- [21] A.B. Khanikaev, S.H. Mousavi, W.-K. Tse, M. Kargarian, A.H. MacDonald, G. Shvets, Photonic topological insulators, Nat. Mater. 12 (3) (2013) 233-239.
- [22] J.P. Lee-Thorp, M.I. Weinstein, Y. Zhu, Elliptic operators with honeycomb symmetry: Dirac points, edge states and applications to photonic graphene, Arch. Ration. Mech. Anal. 232 (1) (2019) 1–63.

- [23] Y.G.N. Liu, P.S. Jung, M. Parto, D.N. Christodoulides, M. Khajavikhan, Gain-induced topological response via tailored long-range interactions, Nat. Phys. 17 (6) (2021) 704–709.
- [24] T. Ochiai, M. Onoda, Photonic analog of graphene model and its extension: Dirac cone, symmetry, and edge states, Phys. Rev. B 80 (Oct 2009) 155103.
- [25] S. Raghu, F.D.M. Haldane, Analogs of quantum-Hall-effect edge states in photonic crystals, Phys. Rev. A 78 (Sep 2008) 033834.
- [26] M.C. Rechtsman, Y. Plotnik, J.M. Zeuner, D. Song, Ž. Chen, A. Szameit, M. Segev, Topological creation and destruction of edge states in photonic graphene, Phys. Rev. Lett. 111 (10) (2013).
- [27] M.C. Rechtsman, J.M. Zeuner, Y. Plotnik, Y. Lumer, D. Podolsky, F. Dreisow, S. Nolte, M. Segev, A. Szameit, Photonic Floquet topological insulators, Nature 496 (7444) (2013) 196–200.
- [28] E. Salete, J.J. Benito, F. Ureña, L. Gavete, M. Ureña, A. García, Stability of perfectly matched layer regions in generalized finite difference method for wave problems, J. Comput. Appl. Math. 312 (2017) 231–239.
- [29] S.V. Tsynkov, Numerical solution of problems on unbounded domains. A review, Appl. Numer. Math. 27 (4) (1998) 465-532.
- [30] E. Turkel, A. Yefet, Absorbing PML boundary layers for wave-like equations, Appl. Numer. Math. 27 (4) (1998) 533-557, Absorbing boundary conditions.
- [31] Y.Q. Zeng, J.Q. He, Q.H. Liu, The application of the perfectly matched layer in numerical modeling of wave propagation in poroelastic media, Geophysics 66 (4) (2001) 1258–1266.
- [32] X. Zhang, Observing zitterbewegung for photons near the Dirac point of a two-dimensional photonic crystal, Phys. Rev. Lett. 100 (Mar 2008) 113903.
- [33] Z. Zhang, S. Liang, F. Li, S. Ning, Y. Li, G. Malpuech, Y. Zhang, M. Xiao, D. Solnyshkov, Spin-orbit coupling in photonic graphene, Optica 7 (5) (2020) 455–462.
- [34] C. Zheng, A perfectly matched layer approach to the nonlinear Schrödinger wave equation, J. Comput. Phys. 227 (2007) 537-556.